Functional and Anatomical Specificity in a Higher Olfactory Centre

Shahar Frechter[1], Alexander S. Bates[1], Sina Tootoonian[1,2], Michael-John Dolan[1,3], James D. Manton[1], Arian Jamasb[4], Johannes Kohl[1], Davi Bock[3], Gregory S. X. E. Jefferis[1,4*]

[1]Neurobiology Division, MRC Laboratory of Molecular Biology, Cambridge, CB2 0QH, UK
[2]Department of Engineering, University of Cambridge, Cambridge, CB2 3EH, UK
[3]Janelia Research Campus, Howard Hughes Medical Institute, United States
[4]Department of Zoology, University of Cambridge, Cambridge, CB2 3EJ, UK

Abstract

Most sensory systems are organized into parallel neuronal pathways that process distinct aspects of incoming stimuli. For example, second order olfactory neurons make divergent projections onto functionally distinct brain areas relevant to different behaviors. In insects, one area, the mushroom body has been intensively studied for its role in olfactory learning while the lateral horn is proposed to mediate innate olfactory behavior. Some lateral horn neurons (LHNs) show selective responses to sex pheromones but its functional principles remain poorly understood. We have carried out a comprehensive anatomical analysis of the *Drosophila* lateral horn and identified genetic driver lines targeting many LHNs. We find that the lateral horn contains >1300 neurons and by combining genetic, anatomical and functional criteria, we identify >150 cell types. In particular we show that genetically labeled LHNs show stereotyped odor responses from one animal to the next. Although LHN tuning can be ultra-sparse (1/40 odors tested), as a population they respond to three times more odors than their inputs; this coding change can be rationalized by our observation that LHNs are better odor categorizers. Our results reveal some of the principles by which a higher sensory processing area can extract innate behavioral significance from sensory stimuli.

Keywords: odor coding; cell types; higher olfactory processing; stereotyped circuits; innate behavior

INTRODUCTION

Activity recordings from single neurons in intact preparations have contributed to many advances in understanding how brains extract behaviorally relevant information from the sensory world. For example in the visual system this approach, combined with carefully controlled stimuli, has identified parallel channels defined by retinal ganglion cells with distinct sensitivities to motion or color (reviewed by Azeredo da Silveira and Roska, 2011) or hierarchical processing of features such as edges in the cortex (reviewed by Hubel and Wiesel, 1998; Priebe and Ferster, 2012). Parallel and hierarchical processing are very general themes of sensory processing; they may depend on cell types or even discrete brain areas specialized to process particular stimulus features or extract higher order percepts. In thinking about the transition from stimulus through perception to behavior, chemosensory systems have become increasingly studied, especially since the identification of odorant receptor gene families in genetic model systems. One reason for this interest is that chemosensory systems appear to be relatively shallow: just two synapses separating the sensory periphery from neurons that are believed to form memories or instruct behavior (Wilson and Mainen, 2006; Masse et al., 2009). It is therefore possible that studies of such chemosensory neurons may reveal general principles relevant to neurons considerably deeper in other sensory modalities.

The olfactory systems of mammals and insects share many organizational features, including the presence of glomerular units in the first olfactory processing center. Second order neurons then make divergent projections onto multiple higher olfactory centers. For example in both flies and mice there there are separate projections to areas proposed to be specialized for memory formation (mushroom body and piriform cortex, respectively) and unlearned olfactory behaviors (LH and e.g. cortical amygdala) (Heimbeck et al., 2001; Jefferis et al., 2007; Sosulski et al., 2011; Root et al., 2014).In insects in general and *Drosophila melanogaster* in particular, the anatomical and functional logic of odor coding in the mushroom body and its relationship to olfactory learning has been intensively studied . About 150 projection neurons (PNs) relay information to the input zone of the MB, the calyx, where they form synapses with the dendrites of ~ 2000 Kenyon cells, the intrinsic neurons of the MB (reviewed in Masse et al., 2009). There is limited spatial stereotypy in these projections (Jefferis et al., 2002; Wong et al., 2002; Tanaka et al., 2004; Jefferis et al., 2007; Lin et al., 2007) and an elegant anatomical approach has found that each KC receives input from an apparently random sample of about 5 PNs (Caron et al., 2013). KC axons form a parallel fibre system intersected by the dendrites of 34 MB output neurons (Aso et al 2014a) and it is proposed that memories are stored by synaptic depression at these synapses. KC odor responses are very sparse (Perez-Orive et al., 2002; Turner et al., 2008), which is proposed to minimize interference between different memories, but do not appear stereotyped across animals (Murthy et al., 2008, but see Wang et al., 2004). Random PN-KC connectivity is consistent with the idea that KC responses acquire meaning through associative learning rather than having any intrinsic valence. In mice, pyramidal cells of the piriform cortex also integrate coincident inputs from different glomeruli (Miyamichi et al., 2011; Davison and Ehlers, 2011), but as in the MB the available evidence suggests that this integration is not stereotyped from animal to animal (Stettler and Axel, 2009; Choi et al., 2011).

In contrast to extensive studies of the MB, there is much more limited information concerning anatomy and function of the LH; this is also true for higher olfactory centers of the mammalian brain that have been hypothesized to serve a similar functional role such as the cortical amygdala. Studies examining the axonal arbors of PNs showed that these have more stereotyped projections in the LH than in the MB (Marin et al., 2002; Wong et al., 2002; Tanaka et al., 2004; Jefferis et al., 2007). Since at least three classes of LH neurons (LHNs) appeared to have dendrites in stereotyped locations (Tanaka et al., 2004; Jefferis et al., 2007), it was hypothesized that these neurons have stereotyped odor responses that are conserved from animal to animal. The first studies of odor responses of LHNs focussed on pheromone responses of neurons suspected to be sexually dimorphic in number or anatomy owing to their expression of the *fruitless* gene (Ruta et al., 2010; Kohl et al., 2013). Kohl et al. (2013) characterized three neuronal clusters showing that they responded in a sex- and class-specific manner and ranged from narrowly tuned pheromone-specialists to more broadly responsive neurons.

Pheromone responsive second order neurons project their axons to a specialized subregion of the LH in both flies and moths (Seki et al., 2005; Jefferis et al., 2007). The extent to which pheromone responsive LHNs are representative of the LH as a whole has been questioned by other studies. In particular Gupta and Stopfer (2012) recorded from a random sample of neurons in the locust LH, reporting that all LHNs were extremely broadly tuned and without finding evidence of neurons with repeated odor profiles; they eventually concluded that generalist LHNs are unlikely to be stereotyped encoders of innate behavior. Fişek and Wilson (2014) carried the first electrophysiological recordings of non-pheromone LH neurons in *Drosophila*. They recorded from two genetically identified cell types with reproducible response patterns: one LHN class responded to 1 out of 8 tested odorants, the other responded to all odorants. Although these results suggested that generalist LHNs can also have stereotyped odor responses, the limit numbered of neurons investigated precluded general conclusions about LH odor coding. Studies of analogous regions in the mammalian brain are even more challenging, but recent recordings by Iurilli and Datta (2017) from the cortical amygdala found no evidence for encoding of the behavioral valence or chemical category of odors or for response stereotypy.

We have taken a stepwise approach to understanding the organizational and functional logic of the LH. We first reasoned that it was essential to characterize the cellular composition of this brain area and to develop approaches that allowed reproducible access to different cell populations. We achieved this by screening and annotating genetic driver lines, analyzing single cell morphologies and using whole brain electron microscopy (EM) data to place rigorous bounds on total cell numbers, which turn out to be much greater than anticipated. We then used single cell electrophysiology to analyze the general principles of odor coding in genetically defined cell populations, finding that LHNs typically respond to more odors but with fewer spikes than their PN input.

Since we find that LHNs show stereotyped patterns of odor activity across animals, we then carry out a detailed analysis of neuronal cell type. We show that functional and morphological criteria can both be used to define cell type and that they are highly consistent. We go on to show that LHNs are better odor categorizers than their PN inputs, providing one justification for their distinct coding properties. We then use EM data to demonstrate direct convergence of different olfactory channels onto both local and output neurons of the lateral horn, providing an anatomical substrate for the response broadening. These results reveal some of the logic by which the nervous system can map sensory responses onto be-

haviorally relevant categories.

RESULTS

Key anatomical features of the lateral horn

Our key goal in this study was to understand the coding principles of third order neurons underlying innate olfactory behaviors. Nevertheless to to understand the functional organization of the lateral horn and the transfer functions that it implements, we felt that it was essential to define some basic neuroanatomical features. There has been extensive analysis of second order olfactory projection neurons providing the main input to the LH (e.g. Marin et al., 2002; Wong et al., 2002; Tanaka et al., 2004; Jefferis et al., 2007; Tanaka et al., 2012a; Costa et al., 2016) with 60 cell types now described (virtualflybrain.org), knowledge of LH local and output neurons was much more limited when we began our studies. We used a wide variety of data types and experimental/analytic approaches over a number of years to obtain a comprehensive overview of the functional anatomy of the lateral horn. We will present those observations most relevant to odor coding here, organized hierarchically (rather than chronologically). However much additional information based on the use of highly specific Split-GAL4 driver lines (Dolan, Frechter et al., in prep) and synaptic resolution EM reconstruction (Schlegel, Bates et al., in prep) will be presented in separate studies.

We begin by measuring volumes of the three main olfactory structures, since neuropil volume is indicative of the energetic investment in particular sensory information (Sterling and Laughlin, 2015) and strongly correlated with length of neuronal cable and synapse numbers (e.g. Schlegel et al., 2017). Using a standard female template brain (Ito et al., 2014, see Experimental Procedures) we find that the first olfactory relay, the AL, has a volume of 1.5×10^5 μm^3. If we normalize other volumes with respect to the AL, the LH and whole MB occupy 65% and 93%, respectively. However while second order projection neurons leaving the AL make synapses throughout the LH, in the MB they are restricted to the calyx region, relative volume 32% or about half the volume of the LH. While third order Kenyon cells are completely intrinsic to the MB, LH output neurons have axonal processes outside the LH. Using light level data, we estimate the amount of LHN arbor outside the LH to be almost exactly the same as the amount within the LH (see Experimental Procedures). It is therefore likely that the complete arbors of third order LHN occupy a greater volume than MB Kenyon cells (130% vs 93%).

The number of neurons carrying information within a brain area is a key determinant of neuronal coding. An early EM study cutting the parallel axon tract of the mushroom body, estimated that there are 2200 Kenyon cells (Technau and Heisenberg, 1982), while studies based on genetic driver lines have counted up to 2000 Kenyon cells (Aso et al., 2009). Previous studies have not attempted to define the number of neurons in the lateral horn, because there is no single tract that can be cross-sectioned in EM, nor any driver line that labels the majority of LHNs. Nevertheless in the locust, Gupta and Stopfer (2012) estimate that there are fewer LHNs than PNs and prevailing estimates in *Drosophila* are in the range 300-500 neurons i.e. 4-7x fewer than the number of Kenyon cells in the MB. We combined light level image data with a new whole brain electron microscopy dataset (Zheng et al., 2017) to address this question. Our screen for LH drivers (see below) identified 30 primary neurite tracts entering the LH. We identified 17 of these tracts (containing 2465 profiles) in the EM volume. A random sampling procedure resulted in an estimate of 1410 LHNs (90% CI 1368-1454, see Experimental Procedures). This number is a lower bound since there are an additional 14 tracts however we believe these contain relatively few LHNs. Since we did not reconstruct complete morphologies for all sampled LHNs, we cannot provide an exact estimate of the proportion of local vs output LHNs. However we do see that each tract consists predominantly of either output or local neurons and on this basis we estimate that there about 580 LH local neurons (LHLNs, 40%) and 830 LH output neurons (LHONs, 60%).

These numbers show that the fly invests a greater neuropil volume in third order LHNs than MB Kenyon cells, arguing for the significance of the LH in sensory processing. Principal neurons of the LH (i.e. third order LHONs) are much more numerous than those of the antennal lobe (second order PNs) and roughly within a factor of 2 of the number of third order MB Kenyon cells. The large number of KCs enables sparse odor coding, which is proposed to avoid synaptic interference during memory formation (reviewed by Masse et al., 2009). Why should the lateral horn also have such a large number of neurons?

Driver lines and hierarchical naming system for LHNs

Transgenic driver lines are the standard approach to label and manipulate neurons in *Drosophila melanogaster* (Venken et al., 2011). Given the large number of LHNs, it seemed essential to identify lines targeting subpopulations to test our hypothesis that LHNs are stereotyped odor encoders.

When we began our studies the only relevant lines came from Tanaka et al. (2004), who identified four drivers labeling distinct populations of LHNs from a screen of about 4000 GAL4 lines. We hypothesized the low yield of this screen was due to a combination of extensive genetic heterogeneity amongst LHNs and the use of classic enhancer trap GAL4 lines, each of which labelled many neuronal classes. With these concerns in mind, we carried out an enhancer trap Split-GAL4 screen (Luan et al., 2006) to generate a more complete and selective set of lines (see Experimental Procedures for details). We eventually selected 270 Split-GAL4 lines containing LHNs (from 2769 screened). These lines enabled us to access the majority of LH cell classes and were used for most functional studies in this paper.

The screening procedure was lengthy and iterative because there was little prior work on LHNs, they are morphologically extremely diverse, and crucially because there was no pre-existing approach to classify and name these neurons. Classification is challenging because in contrast to the antennal lobe or mushroom body, the LH does not contain discrete glomeruli or compartments, which form the basis of neuron naming schemes for those brain areas (Laissue et al., 1999; Tanaka et al., 2008; Aso et al., 2014a). We devised an hierarchical naming system with three levels of increasing anatomical detail to disambiguate neurons (Figure 1F and G): 1) Primary neurite tract, the tract connecting the soma to the rest of the neuron, 2) Anatomy group, neurons of the same anatomy group share a common axon tract and have broadly similar arborizations in the LH and their target areas, and 3) Cell type, this is the finest level – the only difference between cell types of the same anatomy group are reproducible differences in axonal or dendritic arborization patterns that likely reflect specific differences in connectivity. Developing a naming system to classify different LHNs was both essential for successful screening and an important screen outcome.

We chose primary neurite tract as the highest order discriminating factor because each neuron has just one soma and primary neurite tract and because it groups functionally related neurons e.g. those with common neurotransmitters or similar axonal projections. We named the 30 primary neurite tracts found during our screen

based on their anterior-posterior and dorso-ventral position with respect to the centre of the LH: AV1-AV7 (AV=anterior ventral), AD1-AD5, PV1-PV11 and PD1-7. Neurons within each tract typically have a shared developmental origin. Indeed using co-registered image data (Yu et al., 2013; Ito et al., 2013; Manton et al., 2014), we matched neurons following each of the 30 tracts with 39 parental neuroblasts likely to generate LH neurons (Figure S1A) – this indicates that over a third of the neuronal lineages in the central brain have projections in the LH.

Primary neurite tracts can be identified in even quite broadly expressed driver lines, but anatomy group distinctions are not always evident and cell types can usually only be convincingly characterized with single neuron images. We therefore use single cell data to illustrate the distinction between anatomy group and cell type levels (Figure 1G). In our scheme, cell type names are composites incorporating the corresponding tract, anatomy group. Thus cell type PV5a1 belongs to the posterior ventral tract PV5 and anatomy group PV5a. This scheme provides flexibility for the addition of new cell types, while still ensuring that anatomically and functionally related neurons have similar names; this naming strategy may be useful for other brain areas without clearly defined compartments.

Building on our initial screen, we also annotated (Figure 1) the FlyLight (often identified as GMR lines, Jenett et al., 2012) and Vienna Tiles libraries (VT lines, Tirian and Dickson, 2017). These lines are now very widely used in *Drosophila* neurobiology, in part because co-registered 3D image data are publicly available (e.g. through virtualflybrain.org Milyaev et al., 2012; Manton et al., 2014). These lines, which are based on cloned cis-regulatory element GAL4 fusions, were generally more specific than our Split-GAL4 enhancer traps. Similar to our initial screen the vast majority of lines labeled only a few LH anatomy groups (mean of 3) while just 18/448 lines contained more than 7; we did not find even a single line that was specific to multiple LHN anatomy groups without labelling other neurons in the central brain (Figure 1D and E). This demonstrates how hard it is to obtain LH selective lines that label most or even a large portion of the LHNs. At the conclusion of our screen we had identified a total of 72 LHN distinct anatomy groups – ie. neurons with substantially different axonal tracts / arborisation patterns – each of which was consistently labeled by a subset of driver lines. This cellular and genetic diversity significantly exceeded our initial expectations and represented an almost order of magnitude increase over prior studies. Critically it also contrasts strongly with the 7 genetically defined Kenyon cell types in the mushroom body (Aso et al., 2014a).

Besides identifying a small number of additional anatomy groups the GMR and VT annotations also facilitate the construction of highly specific intersectional stocks as well as publicly available hemidriver lines (Dionne et al., 2018; Tirian and Dickson, 2017). We have leveraged these resources to prepare a large collection of Split-GAL4 lines selectively targeting specific LH cell types, which we shall soon report (Dolan, Frechter *et al.*, manuscript in preparation).

Single cell anatomy of the lateral horn

To better understand the cellular composition and functional organization of the LH, we carried out large scale single cell analysis. We collated neurons from FlyCircuit (Chiang et al., 2011) as well as fills of neurons recorded during this study co-registering them all using the approach of Manton et al. (2014) (Figure 2). We segmented these skeletons into axonal vs dendritic compartments (Lee et al., 2014) followed by manual editing based on available confocal stack data and our understanding of neuronal morphology. Based on this segmentation and cross-comparison with the literature, we sorted skeletons into PNs sending input to the LH from first-order sensory neuropils, such as the antennal lobe, or neurons with dendritic arbors in the LH, i.e. LHNs. These co-registered, segmented and annotated 3D skeletons are available for download (github.com/jefferislab/lhns).

We first reviewed LH inputs. 3D atlases of the uniglomerular PNs that provide excitatory olfactory input, have been constructed previously based on co-registration and annotation of single cell data (Jefferis et al., 2007; Costa et al., 2016). Nevertheless, there are numerous additional inputs to the LH. We annotated 1188 LH input neurons and divided them 34 different groups based on the axon tract they use to reach the LH and their pattern of dendritic arborization (Figure S2A). We extended the naming system of Tanaka et al. (2012a) to include 18 types not previously identified (see Experimental Procedures).

We divided LH inputs into functional categories based on the sensory modality inferred from their dendritic neuropil (Figure 2B). Input distribution is not uniform within the LH. Excitatory uniglomerular and inhibitory GABAergic PNs project widely but spare a ventromedial stripe of the LH, which is the focus of multiglomerular olfactory neurons and other sensory inputs; this same arborization pattern is shared by two neuromodulatory neurons releasing octopamine (Busch et al., 2009) and serotonin (Roy et al., 2007). In contrast, excitatory multiglomerular projection neurons are heavily concentrated in the ventromedial LH, where their arbors intermingle with PNs from thermosensory and hygrosensory glomeruli (Frank et al., 2015, 2017); in addition undescribed projection neurons from the Wedge neuropil, may carry mechanosensory wind input (Yorozu et al., 2009; Patella and Wilson, 2018). Gustatory projection neurons also innervate this domain, although these are concentrated in an anterior-medial domain adjacent to the LH (see also Kim et al., 2017). In conclusion, the ventral LH is a site of multi-modal integration while the remainder is purely olfactory.

EM tract tracing presented in the previous section (Figure 1) estimated that the lateral horn contains ~1400 neurons. What is the anatomical and functional diversity amongst this large number of neurons? We assembled a library of 1172 light level skeletons that innervate the LH (plotted in Figure 2C left, see Experimental Procedures).We assigned neurons to anatomy groups and cell types (Figure S2B) using NBLAST clustering (Costa et al., 2016) followed by close manual review (Figure S2B′). The definition of cell type was based on the range of NBLAST clustering cut heights previously used to define other cell types in the fly brain (Costa et al., 2016) and assessment of the level of within and across cell-type stereotypy in fine branching patterns. In spite of the use of sophisticated computational anatomy, we find that there is no unique statistical definition for anatomical cell types, even when these can be validated by other cellular properties (see below). Nevertheless for those cell types with more than one neuron, NBLAST identified the correct cell type ~ 80% of the time (Figure S2E).

We found 47 cell types with arbors restricted to the LH, which we took to be local neurons (LHLNs); we also found 127 cell types with arbors both within and beyond the LH, which we classified as candidate LHONs. Although these cell types originate from all 31 primary neurite tracts, most originate from the tracts identified by EM as containing the largest number of LHNs (Table 1). Both the EM data and analysis of light level skeletons indicated that LHLNs belong to a much smaller number of primary neurite tracts (two large ones: AV4 and PV4 account for more than 2/3 of the estimated 580 local neurons). Nevertheless there is significant diversity within these groups; for example the AV4b and PV4b anatomy

groups include morphologically similar neurons that appear to make short range output to the superior lateral protocerebrum (SLP) (Figure S3A-A'). Without information about synapse placement it is hard to be certain if these are polarized neurons with axonal arbors in the SLP or local neurons whose domain extends somewhat beyond the anatomically defined LH.

LHONs originate from a larger number of tracts and have many more cell types, consistent with a wide range of axonal projections. We measured the mean amount of cable each LHON cell type contributed to each standard neuropils (Ito et al., 2014) (Figure 2E). Given the surprisingly large number of LH associated cell types, we defined a set of core LHONs, that clearly had significant dendritic arborization in the LH. 60 LHONs met criteria based on the having >15% of their dendrites within the LH and ample overlap with PN terminals (Figure S2F; seeExperimental Procedures for details). These LHONs have a wide array of target neuropils (Figure 2E) with the super protocerebral neuropils (SLP, SMP and SIP) being the most extensively innervated along with the ventrolateral protocerebrum (AVLP, PVLP). Superior protocerebral areas include convergence zones where direct olfactory output from the LH may be integrated with learned olfactory information from the mushroom body (Aso et al., 2014a); the ventrolateral protocerebrum, which also receives extensive input from visual projection neurons originating in the optic lobes (e.g. Panser et al., 2016). Additional targets include other regions of the superior protocerebrum including clamp and crepine; finally some neurons have both axonal and dendritic domains in the LH. Few cell types project to the contralateral hemisphere, perhaps because most olfactory projection neurons in the adult fly already receive information from both antennae.

Odor Responses of Lateral Horn Neurons

Having described core features of lateral horn anatomy and identified appropriate genetic driver lines, we can now address the principles of odor coding in the LH. Our basic goal was to define the odor response properties of LHNs and to compare them with their presynaptic inputs, the PNs. We also hoped to contrast LHN responses with those of MB Kenyon cells, the other main class of third order olfactory neuron. Given that these cells had unknown response properties and our previous experience was that calcium signals in LHN somata are not a sensitive measure of LHN firing, we carried out *in vivo* whole cell patch clamp recordings using the approach that we have previously described (Kohl et al., 2013). We recorded 587 cells of which 410 (242 LHONs, 84 LHLNs, and 84 identified PNs) reached the criteria for inclusion in our population analysis (see Experimental Procedures). When we compared basic electrophysiological parameters across different groups we saw that both LHONs and LHLNs generally had a much higher input resistance and lower cell capacitance than PNs (Figure S4D); this suggests that the energetic costs of individual spikes in LHONs than their PN inputs.

We selected an odor set designed to excite many different olfactory channels (Hallem and Carlson, 2006; Münch and Galizia, 2016) that included diverse chemical groups including acetates, alcohols, organic acids, aldehydes, ketones, amines and phenyls. Our core odor set consisted of 36 odors (Figure 3B) although up to 53 odors were used for some cells in the study. In general LHONs showed little spiking in the absence of odor. This was in contrast to PNs which showed higher baseline firing rates (Figure 3A and C) consistent with previous reports (e.g. Wilson et al., 2004) . The baseline firing rate of LHLNs was intermediate. Odor responses were reliable for all 3 groups and it was very rare for a cell to have an appreciable response to one odor presentation without responding to the other presentations of the same odor.

Comparing the number of odors that elicited a significant response for the 3 groups we see that LHONs respond to more odors then both PNs and LHLNs (Figure 3C). When we compare the firing rate across the full set of odor responses the firing rate was similar between PNs, LHLNs and LHONs. However taking into account that PNs (and LHLNs) responded significantly to fewer odors then LHONs and that the baseline firing rate was different between the 3 groups it is also informative to compare the firing rate in the significant (excitatory) responses. Comparing significant responses only we see that LHONs respond with a lower firing rate (but to more odors) Figure 3C.

To conclude we see that on average LHONs are 10x quieter than PNs at baseline, show significant responses to 3x more odors, but have lower evoked firing rates, therefore firing a similar total number of spikes.

Defining LHN physiology classes by odor response

As we carried out our recordings, it became apparent that cells regularly fell into distinct groups based on their odor tuning profile. For example neurons from the same anatomy group could respond quite differently from one another. We were particularly interested in the finest level of classification or cell type and whether anatomical or odor tuning differences would individually be sufficient to define cell types. We use the term *physiology class* to define cell types separated at this finest level of classification by their odor response properties

Although it might have been desirable to assign physiology class based only on functional data, we decided to begin by separating neurons using coarse anatomical features (primary neurite tract, axon tract). We consider that this is justified philosophically both because neuronal morphology at this level results in groups that neuroanatomists agree correspond to distinct anatomical types and because all anatomy groups can be distinguished by the expression patterns of discrete genetic driver lines.

At a more practical level, there are many LHONs that have rather similar response properties. For comparison, PNs are generally assumed to be highly stereotyped odor responders, but we found that many PNs were not perfectly clustered using functional data alone.

We decided to classify neurons manually and use automated methods to validate our approach. In total we manually annotated 70 unique physiology classes, of which 52 contain two or more exemplars. Hierarchical clustering presented in Figure 4A, clearly separates some classes of LHONs and LHLNs, but many classes do not co-cluster perfectly. It makes intuitive sense to first identify PNs by their glomerular innervation in order to form functional groups. We turned again to our only clear unitary anatomical feature for LHNs, the primary neurite. Automated clustering does a reasonable job in identifying our manually defined physiology classes, using cells classified in the context of their primary neurite tract. In all cases but one (AD1) the classes were correctly identified with just 1-3 errors (i.e. cases were cells of the same class did not co-cluster) and an adjusted Rand index in the range of 0.5-0.75 (Figure 5D). While we could not correctly identify all cells within each class, it does suggest that our our manual classification strategy is well grounded, and supports our interpretation that there are many separate LHN classes.

Many of the lines in the first round of screening contained several distinct physiology classes Figure S1B. While some classes were very obvious with minimal variability in odor responses (Figure 4E'), others were less easily identified (Figure 4E"). In particu-

lar, we regularly observed that the common odor response profile of cells of the same class was masked by significant differences in response magnitude or threshold. This may originate from differences in the number or strength of inputs to that cell type within or across animals. Given that we recorded from one cell per animal, we cannot exclude variation due to experimental noise, i.e small differences in fly location. However we did not find any consistent relationship between cell-recording parameters (cell capacitance, membrane resistance and pipette resistance) and the strength of the response, suggesting that this is not an artifact of recording conditions (Figure S4). Furthermore recent analysis (Fig 6A of Dolan et al., 2017) of new whole brain EM data (Zheng et al., 2017) suggests that LHNs of the same cell type within one animal can receive varied numbers of PN inputs that could well account for the observed response differences.

Fine scale anatomical clustering confirms LHN classification

In order to further validate our physiology classes by an independent way we turned to anatomy. A significant fraction (147/326) of our recorded LHNs were traced and registered Figure S3B allowing us to compare the classification by physiology to the anatomy of the cells. As can be seen although the anatomy classifier is not without mistakes. It is evident that there is a clear match between the physiology type and the cell anatomy Figure 5B. In general automatic classification by anatomy was in many cases better than automatic classification by physiology, that is although the original cell class definition is by physiology. This result generally confirms our cell classification approach. Also this result confirms our observation that cells may belong to the same physiology class (cell type) may vary significantly in their response strength .

What is the reason cell physiology underperformed in comparison to cell anatomy? We think this is the result of a few contributing factors

1. High correlation between responses of cells that belong to different physiology classes (see below) .
2. Variation in response strength between cells that belong to the same class.
3. Physiology clustering is limited to 36 odors only. While this a large number by experimental standards, it is still a fraction of the odor space flies are likely to encounter.

In only one case (PD2) the physiology classification performed significantly better then anatomy classification Figure 5D and see also Figure S5A. Classes 12 and 14 were routinely clustered together both by physiology and anatomy and class 28 was clustered apart by physiology in this specific example. These cells belong to cluster PD2a1/b1 and were identified as post synaptic to MBV2/MBON-α2sc and were shown to change their odor response according to the experience of the fly. We therefore decided to combine these classes as there is a strong possibility that in this specific case the difference in response properties is the result of different input from the MBON-α2sc neuron

In a couple other cases both anatomy and physiology automatic classification were not fully in agreement with our own manual classification we reanalyzed carefully both the physiology and anatomy of the relevant clusters in detail. In one case (classes 34 and 35) there seem to be a significant difference in response strength or threshold while anatomy of the cells was very similar Figure S5B. Genetically these classes seem to appear in the same lines Figure S1B with no strong preference (not statistically verified). As we suspect that in some cases cells of the physiology class might have very different response strength we decided to combine these classes to one class(34) for further analysis. In the other case there are clear physiological and anatomical differences between the classes that were overlooked by the classifier Figure S5C. Having corrected these classes the results of the anatomy classifier has significantly improved (without using PD2 as there are now too few classes) Figure 5E and see also Figure S5D.

Altogether our results support a view in which the LH is composed of many cell types (in the order of hundreds) with stereotyped odor responses (with the exception of PD2a1/b1 and maybe a few other exceptions). We also find a high variability in the response strength of cells of the same class and a high level of odor response correlation between many classes of LHNs, both sometimes leads to misclassification.

LHONs sample odor space in a non homogeneous manner

When we compare the heatmaps of PNs, LHLNs, and LHONs we notice that they look quite different (Figure 4A-B). The overall response correlation is significantly higher for LHONs then both PNs and LHLNs. Also PNs and LHLNs heatmaps are “clean” with hardly any off diagonal structures while LHNs heatmap is much more complex. These 2 differences are obviously not independent of each other as the higher the overall correlation across the population you are more likely to have off diagonal structures. We therefore combined the analysis of both these changes and considered three options as the origin for the differences we see between PN and LHONs heatmap.

1. LHONs sample the odor space in a biased manner pooling the same odors together in different classes leading to higher correlation -Odor space.
2. LHONs are broader and respond significantly to more odors. The broader the cells they are more likely to be more correlated with other cells, therefore it is possible that broadening of the odor response is the source of the increased correlation - Sparseness.
3. There are more LHONs then PNs. This is true both if we consider our current estimates for cell numbers or if we consider our dataset only. As the number of cells and cell types sampling the same odor space increase, differences between the types sampling the same space are bound to get smaller and therefore some groups are inevitably more similar to other groups - Class number.

The first possibility we will consider is that LHONs sample the odor space in a biased manner pooling the same odors together in different classes leading to higher correlation between those classes. One way to compare how well the different cell populations are sampling the odor space is by randomizing their odor labels Figure 6A. This way we are not affecting the general firing rates or sparseness distribution but only the correlation between different odors across the classes. If cells (and classes) are sampling the odor space efficiently (i.e as homogeneously as possible) as a population then randomizing the labels should not significantly affect the correlation distribution. If however the sampling is not efficient and odors are pooled together similarly in different classes then randomizing the labels should significantly reduce the correlation.

To analyze this possibility we first aggregated our data by class and calculated the mean odor response for each physiology class . This was done to control for differences in the number of cells per class. We then randomized the odor labels and calculated the correlation shift i.e the mean correlation minus the mean correlation

of the randomized heatmap for each group. Indeed we see Figure 6D that randomization has a much stronger effect on LHONs then PNs demonstrating that LHONs indeed sample the odor space less homogeneously. This also suggest that neither the number of LHON physiology classes in our dataset nor the broadening of the response in LHONs are enough to explain the increased correlation in LHONs.

We next wanted to test wether broadening of the odor response is the source of the increased correlation in a more direct manner. To do so we compared the mean correlation by class. Indeed as we hypothesized there is a correlation between the mean response probability and the mean correlation of a class . However we clearly see that when compared against PN classes of similar sparseness LHONs show higher correlation (Figure 6E).

One caveat to this approach is that across the population LHNs are broader. Therefore each class (including the sparse ones) was compared in the case of LHONs against a significantly broader class. To avoid this shortcoming we limited our analysis to sparse classes only (red line in Figure 6E') to avoid comparison of sparse classes to much broader classes in LHON Figure 6F. Again LHONs were more correlated then PNs. This also demonstrate again that the number of classes are not the main reason for the high correlation as by limiting our analysis to sparse classes only we also matched the number of PN and LHON classes (20 and 22 respectively).

Altogether we therefore conclude that LHONs sample the odor space less homogeneously than PNs leading to higher correlation in LHONs and further shows that increased breadth of LHONs or the increased number of LHON classes are not the main reason for the high correlation.

Encoding of odor categories

We have already explored a number of aspects of odor coding by LHNs. For example we have seen that LHNs respond to 3 times more odors than their PN inputs and that they sample odor space inhomogeneously. We hypothesized that these features of LHN odor coding arise because they pool specific odor input channels that signify odors of common behavioral significance. Although the issue of valence has received considerable attention recently (reviewed by Knaden and Hansson, 2014), results are extremely dependent on the exact behavioral paradigm and odor concentration used. Therefore rather than trying to examine LH odor coding from the perspective of the valence reported for different odors in the literature, we initially focussed on encoding of chemical features. We categorized our odor set based on the presence of alcohol, aldehyde, amine, carboxyl, ester, phenyl chemical groups.

We first examined odor encoding at the population level of PNs, LHLNs and LHONs using principal components analysis. The first principal component consistently encoded response magnitude. Figure 7A shows the population response trajectories for projected into the space of the second and third principal components, and color-coded by odor category. Two features of this analysis seemed particularly noteworthy. First, there was a progressive increase in how spread out odor representations were in this principal component space. Second, LHON responses appeared to separate certain odor categories, especially amine containing odors (typical of decomposing biological matter) versus acetates (typically light, fruity odors).

This result motivated us to examine the ability of individual LHNs to encode odor categories. We took each cell to be a binary classifier for a given odor category, i.e. signaling the presence or absence of the category and measured its performance using a normalized area under the ROC curve (AUC) score (see Experimental Procedures). Figure 7B indicates that LHONs but not PNs convey category information in their odor responses, when compared with a shuffled control distributions. The LHON population has the largest fraction (70%) of category-informative cells, followed closely by LHLNs, which have nearly twice as many category-informative cells as PNs. (Figure 7B). LHONs had a particularly large fraction of amine categorizers (almost 45% of cells) but also had selective neurons for all 6 categories (Figure 7C). These results indicate that LHNs indeed develop a novel ability to encode higher order odor features that are more likely to be behaviorally relevant to the fly, confirming a longstanding hypothesis in the field.

As noted earlier, PCA analysis suggested that odor responses were increasingly spread out when examined in moving from PN to LHON population responses. This likely occurs because LHONs pool inputs from multiple odor channels resulting in a greater spread within the higher rank principal components. We tested this intuition by measured the dimensionality of the neural representation using the approach of Abbott et al. (2011). This measure yields a value between 1 (all the variance is explained by a single component) to $d = N$ (each component explains an equal fraction of the variance). In Figure 7E we plot the dimensionality of odor representations by population compared with shuffled controls. Shuffling odor labels tends to spread out the odor representations, yielding a higher estimate of the dimensionality, as expected. The unshuffled populations appear to have the same dimensionality. However, our measure is sensitive to the size of each population. To account for this, we recomputed dimensionality after randomly subsampling the different populations to equalize population sizes. When the difference in population sizes is accounted for (Figure 7E') the LHON representation indeed has a lower dimensionality than both the PN and LN representations. These results confirm our earlier analysis of the population response heatmaps (Figure 6).

Integration of odor channels by LHNs

Many of our observations (increased tuning breadth, increased single cell categorization ability, reduced representational dimensionality) suggest that the LHONs pool olfactory information to better inform the behavioral significance of an odor. Although this provides a rationale for the observed differences in odor coding, it does not account for them mechanistically. Previous light level studies have attempted to predict PN to LHN connectivity (Jefferis et al., 2007) and one physiological study directly validated the convergence of two different PNs onto a specific LHN class (Fişek and Wilson, 2014). However the first approach can only describe potential connectivity, while the second was restricted to a subset of the possible inputs to just one LHN class.

In order to compare our observations about LHN odor coding with measurements of the PN to LHN convergence ratio, we leveraged a newly available whole brain EM dataset (Zheng et al., 2017). This allowed us to obtain direct information about how LHN dendrites integrate inputs from different PN axons. These data build on our recent analysis of PN input to LHONs of the PD2a1/PD2b1 cell types (Dolan et al., 2017). We selected an anatomically diverse sample of 13 LHONs and 6 LHONs, derived from 7 and 4 primary neurite tracts, respectively. We analyzed the complete repertoire of excitatory PN input onto their dendrites originating from 51 glomeruli (see Experimental Procedures).

All neurons analyzed had a small number of strong inputs but most had a long tail of weaker inputs. Therefore although they received at least one input from 14 glomeruli on average (range 3-21), if we considered only those glomeruli accounting for more than 3%

of the total PN input to a given LHN, then LHNs received 3.2±1.4 significant glomerular inputs (mean ± standard deviation). There was a trend for LHLNs to receive fewer inputs (2.5 vs 3.5) but this difference was not significant for this relatively small dataset. These numbers provide a key parameter to start modeling the circuit origins of the odor coding properties of LHNs. They are also comparable with recent observations based on optogenetic mapping of PN-LHN functional connectivity (R. Wilson and J. Jeanne, personal communication).

DISCUSSION

Odor coding in LH

Our principal finding is that LH output neurons (LHONs) as a population are genetically and anatomically defined cell types with stereotyped odor responses. Starting from recordings of genetically defined populations we cross-validated fine scale anatomical differences and odor tuning for 37 LHN cell types; this confirms that stereotypy is a general feature of the LH and not particular to specialist odor pathways such as those that process pheromone information, which may retain a labeled line logic all the way from the periphery. Although we see evidence of narrowly tuned LHNs dedicated to the processing of specific odors, the population as a whole shows 3x more odor responses than their PN inputs. The increased tuning breadth may reflect a transition to a more behaviorally relevant coding scheme. This is consistent with our findings that LHNs show significantly improved odor categorization compared with PNs apparently from stereotyped pooling of related odor channels. The chemical categories that we analyzed are probably not of direct ethological relevance to the fly, but serve as proxies – further explorations of olfactory neuroecology are clearly necessary. For example we saw limited evidence for simple representations of olfactory valence in LHN responses.

It is instructive to compare the odor tuning properties we find across the lateral horn with those reported for the *Drosophila* mushroom body. Major differences in the MB include the lack of response stereotypy (Murthy et al., 2008) and sparser odor tuning (Turner et al., 2008); the distribution of odor tuning in the LH also appears to be wider – i.e. LHNs appear more functionally heterogeneous. However, there are also similarities – there is divergence of PNs onto a larger population of third order neurons in both cases. Furthermore baseline firing rates are very low in both LHNs and Kenyon cells and the evoked firing rates are also lower than in their PN input. This could reflect energetic, spike economy considerations or a need to binarize neural responses prior to memory formation or organizing behaviors.

It is also interesting to compare response properties with recent recordings from the mammalian posterolateral cortical amygdala (Iurilli and Datta, 2017), which has been compared to the LH, since it receives spatially stereotyped input from the olfactory bulb (Sosulski et al., 2011)and is required for innate olfactory behaviors (Root et al., 2014). (Iurilli and Datta, 2017) found that odor tuning properties were very similar to the mammalian piriform cortex (which has been compared to the mushroom body). Both regions showed decorrelated odor representations (whereas we find that LHN odor responses show significant correlations suggestive of a focus on particular combinations of olfactory channels) and odor tuning in the cortical amygdala was actually somewhat sparser. In further contrast to our observations in the LH they found no evidence for categorization of odors by chemical class and crucially no evidence for response stereotypy, in a way suggestive of stereotyped integration of defined odor channels. We would however caution with respect to the last point that recording a small fraction of randomly selected neurons from the *Drosophila* LH could easily miss response stereotypy. It is only because we were able to use genetics to bias our sampling, and also to record from a significant fraction of the whole LH population, that we could obtain clear evidence for odor response stereotypy. Nevertheless, these differences seem marked and it will be very interesting to compare the logic of these systems across organisms. One point to note is that the circuits in the fly may be more compact with LHNs, in a few cases connecting directly to fourth order neurons with descending projections to the nerve cord likely to have a direct impact on behavior (Ruta et al., 2010, ; Huoviala et al., in preparation).

Circuit mechanisms

There are some similarities between the increase in tuning breadth that we observe at the PN-LHN transition and what has previously been reported at the first synaptic layer of the olfactory system (the olfactory receptor neuron to PN synapse). In the antennal lobe broadening appears to depend on a compressive non-linearity, which boosts weaker inputs Bhandawat et al. (2007) and possible excitatory local interactions (Olsen et al., 2007; Shang et al., 2007). Although a direct comparison between the extent of broadening in the antennal lobe and LH is not possible without measuring odor responses from many receptor neurons under the same stimulus conditions (as we did for PNs and LHNs) it seems likely that the effect is larger in the LH. Importantly the mechanism here appears quite different, with direct pooling of feed-forward inputs.

Our initial EM connectomics observations suggest that a typical LHON receives strong inputs from 3-4 excitatory PNs albeit with a long tail of weaker connections, some of which are likely to have an impact. Intriguingly this number (referred to as the synaptic degree, K, Litwin-Kumar et al., 2017) is not that different from the 7 inputs reported for Kenyon cells in the mushroom body (Caron et al., 2013). However the rules of integration must be quite different, because they result in broadening in LHONs and a sharp reduction in tuning breadth in KCs. How is it that LHONs and KCs listen to the same information but produce very different responses? Fişek and Wilson (2014) and Gruntman and Turner (2013) have, respectively, proposed that in *Drosophila* both LHNs and KC dendrites linearly integrate their inputs. The differences could result from both intrinsic and circuit mechanisms (i.e. local interneuron interactions), but two factors likely to have a major impact are the spatial distribution of synapses and the spike threshold. PN inputs are broadly distributed across LHON dendrites (Schlegel, Bates et al, in preparation), whereas PN inputs onto KCs are highly clustered at individual dendritic claws. The many individual connections at each KC claw may be integrated to produce a reliable response that is nevertheless usually below the spike threshold – therefore multiple input PNs must be co-active and KCs act as coincidence detectors. In contrast the inputs on LHON dendrites may be integrated in a more graded fashion with a lower spike threshold (Fişek and Wilson, 2014). Of course the biggest difference is that LHNs receive stereotyped inputs according to their anatomical/genetic identity (see Dolan et al., 2017) and this provides a mechanism for the odor response stereotypy that we observe.

We would also like to highlight some additional differences in circuit architecture between the MB and LH that may be of functional significance. First the MB calyx receives only excitatory PN input, whereas, there a population of almost 100 inhibitory PNs that project to the LH . Second we find that the LH contains an estimated 580 local neurons (most of which are inhibitory, Dolan, Frechter et al, in preparation), whereas the mushroom contains just

one local inhibitory neuron, the APL. We suspect that a major reason for this difference is again related to the stereotyped vs non-stereotyped design of these two centers. The APL is not selective but appears to pool all KC inputs to implement a winner take all gain control mechanism, suppressing more weakly activated KCs (Papadopoulou et al., 2011). Our preliminary EM results show that at least some LHLNs integrate small numbers of input channels (2-3 strong inputs). We suggest that they then make stereotyped connections either reciprocally onto their input PNs or onto other specific neurons in the LH.

Cell types in the central brain

There is renewed interest in the identification of cell types in the brain as an important step in the process of characterizing circuits and behavior (Zeng and Sanes, 2017). Historically, cell types have been best classified by morphology and the most detailed work has been in the sensory periphery (e.g. 55 cell types in the mouse retina: Masland, 2001). Recently single cell transcriptomics has begun to match this morphological classification (Shekhar et al., 2016) and also to enable more detailed exploration of diversity in deeper brain regions (e.g. 49 cell types in mammalian cortex: Tasic et al., 2016). However, relating cell types to functional and network properties especially in higher brain areas remains challenging.

One of the major surprises from our work is our conclusion that there are at least 107anatomically distinct cell types in the LH; given our cross-validation of anatomical and odor response properties for 37 lead us to believe that most of these will turn out to be functionally stereotyped as well. Furthermore we know that we have not identified all anatomical cell types in the LH and we estimate that there should be >250 specific cell types amongst the >1300 LHNs. This raises a number of issues with respect to cell types.

One interesting observation that we made that is that it was easier to identify cell types anatomically than by odor response profile alone. It has recently proven possible to characterize 30 retinal ganglion cell types in the mouse based solely on their visual response properties (Baden et al., 2016). It visual stimulation protocols with odor delivery; although our core 36 odor set was large by the standards of the field, this is still a small fraction of the world of possible odors for the fly. Nevertheless there appear to be many more LHNs than retinal ganglion cell types and we find examples of neurons that appear to be solely distinguished by their projection patterns (presumably defining different downstream partners) which are only revealed through anatomical characterization. For these reasons we believe that response properties alone are insufficient to define cell type and this seems likely to be the case in other higher brain areas.

Preliminary evidence from EM connectomics (Figure 7E; Dolan et al., 2017) suggests that specific LHN cell types integrate stereotyped sets of olfactory channels. It will be exciting to integrate functional and anatomical properties more deeply with circuit properties. Furthermore the genetic screening that we describe identify at least 72 genetic profiles based on expression of driver lines. The existence of such a rich and coupled anatomical diversity raises interesting questions about how connection specificity can be achieved during development.

What is the behavioral function of the lateral horn?

The lateral horn has is one of two major olfactory centers in the fly. The hypothesis that it might play a specific role in unlearned olfactory behaviors dates back at least to Heimbeck et al. (2001). This has been strengthened by observations about the relative anatomical stereotypy in input projections to the mushroom body and lateral horn (Marin et al., 2002; Wong et al., 2002; Tanaka et al., 2004; Jefferis et al., 2007; Caron et al., 2013). Nevertheless in spite of this general model of a division of labour between LH and MB, functional evidence has been hard to come by. Some arguments about LH function have been based on experiments that manipulate mushroom body neurons; here it is worth noting that there are olfactory projections neurons that target areas outside of these two principal centers (e.g. Tanaka et al., 2012a; Aso et al., 2014b) so the lateral horn cannot rigorously be concluded to mediate behaviors for which the mushroom body appears not to be required.

In this experimental vacuum a large number of hypotheses have been proposed for LH function. One obvious suggestion based on anatomy was that LHNs should integrate across olfactory channels (Marin et al., 2002; Wong et al., 2002). Of course integration can have opposing effects on tuning. For example Luo et al. (2010) proposed that LHNs might have highly selective odor responses and early recordings from narrowly tuned pheromone responsive neurons are consistent with this idea (Ruta et al., 2010; Kohl et al., 2013). However Kohl et al. (2013) also observed more broadly tuned neurons that clearly integrated across olfactory channels and Fişek and Wilson (2014) were able to show quite linear integration of two identified olfactory channels. Our electrophysiological recordings together with first EM connectomics results suggest that integration across multiple odor channels and broadening of odor responses are the norm.

Turning to the biological significance of LHNs for the fly. One suggestion based on anatomically discrete domains for food and pheromone odors was that the LH might organize odors by behavioral significance (Jefferis et al., 2007). Others have suggested that the LH might mediate innate responses to repulsive odors only (Wang et al., 2003) or that the LH might organize odor by information by hedonic valence (Strutz et al., 2014). Although our survey of LHN odor responses is not yet conclusive on any of these points, we did find clear evidence for an improved ability to categorize chemical groups of odorants (Figure 7). Further work integrating more information about the behavioral significance of different odors should be instructive.

One synthesis of these different ideas is that the mushroom bodies perform odor identification, whereas the lateral horn/protocerebrum performs odor evaluation (both learned and innate)(Galizia, 2014). Although we have no evidence to support a direct role for the LH in evaluation of learned olfactory signals, new work from our group has identified a class of lateral horn neurons that integrates both innate (directly from the antennal lobe) and learned olfactory information from MB output neurons of specific valence; these LHNs are required for innate appetitive behavior as well as learned aversion (Dolan et al., 2017). We have also identified LHN axon terminals as targets of mushroom body output neurons suggesting that mushroom body modulation innate olfactory pathways may be a general strategy of learned behavioral recall (Dolan, Frechter et al. in preparation).

To return to a key question posed at the start of the manuscript: why does the LH need so many cells and cell types? At this stage we would suggest that LHNs are likely to show both stereotyped selectivity for odor categories and specificity for different aspects of odor-guided behavior. Specific combinations of the same odor information could be used to regulate distinct behaviors by targeting different premotor circuits. We have recently identified a requirement of a specific LHN populations in select aversive olfactory behaviors to the toxic mold odorant geosmin (Stensmyr et al., 2012, ; Huoviala et al. in preparation). The picture that this paints is of a complex switchboard for olfactory information. it seems likely that different paths for the information flow through the LH may be mod-

ulated by external signals such as the internal state of the animal (Galizia, 2014; Wang et al., 2013). We believe that the next few years should see very rapid progress in understanding the logic of circuits within the LH and their downstream targets through the impact of connectomics approaches combined with the characterization that we have begun in this study. In conclusion, we believe that the *Drosophila* lateral horn offers a very tractable model to understand the transition between sensory coding and behavior.

EXPERIMENTAL PROCEDURES

Split-GAL4 screen

We hypothesized the low yield of previous screens to identify LH driver lines was due to a combination of extensive genetic heterogeneity amongst LHNs and the use of classic enhancer trap GAL4 lines, each of which labelled many neuronal classes; if an expression pattern labels many neurons, expression in a small subpopulation may be missed either because they are obscured by brighter neurons or because neurons of interest do not have a common highly organized structure that observers can more easily discern (Ito et al., 2003).

With these concerns in mind, we carried out a Split-GAL4 screen (Luan et al., 2006) to generate a more complete and selective set of lines. Split-GAL4 driver lines achieve their increased specificity by the use of two hemidrivers, enhancer trap activation domain lines (ET-AD) and the other for enhancer trap DNA binding domains lines (ET-DBD), each of which must be co-expressed within a cell in order to reconstitute a functional transcription factor. The first stage of our screen was only designed to identify ET-AD and ET-DBD lines that are enriched for LHNs. At this stage we only rejected expression patterns that were either very broad with strong expression across the brain, or contained no labelling at all in the LH. Any line that passed this basic check was then stained and imaged at high resolution on a confocal microscope allowing LHNs to be identified and annotated amongst complex expression patterns.

Split-GAL4 screen: DBD and AD enhancers lines were crossed to broadly expressing lines (UAS-CD8-GFP ; UAS-CD8-GFP; elav-AD and UAS-CD8-GFP ; UAS-CD8-GFP; Cha-DBD respectively) and visualized by the expression of mCD8-GFP (Lee and Luo, 1999). Lines were selected and annotated based on expression patterns. At the second stage of the screen lines that had similar clusters were crossed and the final expression pattern evaluated and the best lines in terms of specificity and strength of expression were selected for electrophysiology. As we carried out the physiology screen using lines generated in our lab, them GMR and VT lines became available for screening. As these lines were sometimes sparse enough to be used directly for physiology we selected some GMR lines for recording as well.

ET-AD insertions were screened by crossing to Cha-DBD (in theory targeting cholinergic excitatory neurons) with a GFP reporter, while ET-DBD insertions were crossed to elav-AD (in theory targeting all neurons). In each case the resulting expression pattern was imaged. Of these lines we chose the best lines based on criteria such as selectivity, and expression strength. The expression pattern was analyzed and annotated for selected lines. Image registration (Ostrovsky et al., 2013) to the standard IS2 template brain (Cachero et al., 2010; Manton et al., 2014) was used to facilitate comparison of lines and clusters. AD and DBD lines that potentially contained the same neurons of interest were then intercrossed to generate more specific lines.

Computational Neuroanatomy

Open source neuron skeletons were obtained from `http://www.flycircuit.tw/` (accessed: January 2017), filtering for any skeleton with processes in within the LH (total: 2192). These skeletons had been automatically reconstructed from sparse image data and the dataset described in previous studies (Chiang et al., 2011; Lee et al., 2012). A bridging registration Manton et al. (2014) was generated from their Standard Model Brain to our FCWB template brain using the Computational Morphometry Toolkit (`https://www.nitrc.org/projects/cmtk/`). Skeletons manually traced from successfully dye-filled neurons () during physiological experiments were also registered to a template brain (IS2, Cachero et al., 2010) and bridged into the same FCWB space so that all skeletons could be directly compared. NBLAST clustering of skeletons that, upon visual inspection, seem that they should belong to the same cell type but come from these two different origins segregates skeletons based on cell type first, then origin (Figure S2B). Skeletons were then assigned as possible PN inputs (1149) to the LH from sensory neuropils or LHNs (1172). A minority (1149) of skeletons seemed to input the LH from other brain areas, for example known MB output neurons (Aso et al., 2014a) and others that may be centrifugal inputs from other brain areas. Lacking synaptic data we excluded them from our analysis. Skeletons where split into axonal and dendritic compartments based on a classifier trained on skeleton data from the *Drosophila* medulla Lee et al. (2014) followed by manual editing based on available confocal stack data and expert understanding of neuronal morphology.

The most studied projections to the LH are GH146-GAL4 positive, excitatory uniglomerular projection neurons from the antennal lobe (AL) that run through the medial antennal lobe tract (mALT). Tanaka et al. (2012a) have described five types of mALT, three types of mediolateral antennal lobe tract (mlALT), three types of lateral antennal lobe tract (lALT) and three types of transverse antennal lobe tract (tALT) PNs that project to the LH from the AL. PNs taking either tract can have uniglomerular, multiglomerular or non-glomerular dendritic arborisation in the AL, sampling broadly or sparsely from the available odor channels. Unlike Tanaka et al. (2012a), but as has been observed in the larva (Berck et al., 2016), we find that some of these mALT olfactory projections do not arborize in the MB calyx (data not shown). GABAergic olfactory input is known to be supplied via PNs traversing the mlALT (Wilson and Laurent, 2005; Okada et al., 2009), whereas the majority of projections through the mALT and lALT are thought to be cholinergic (Tanaka et al., 2012a). We were not able to find a few PN types that had been described in the literature to project to the LH, including AL-MBDL (Tanaka et al., 2012a). As well as olfactory input, other sensory modalities including second order gustatory and thermosensory (Frank et al., 2015) projection neurons target the general area of the LH. However these have not yet been extensively characterized nor compared in detail with olfactory projections. Neuromodulatory neurons also target the LH, including those releasing octopamine (Busch et al., 2009) and serotonin (Roy et al., 2007). We were able to identify examples of these categories in the FlyCircuit dataset, as well as projection neurons originating from the Wedge that may be wind sensitive (Yorozu et al., 2009). Due to sampling biases in the FlyCircuit dataset, it is very likely that some cell types are over-represented, while others may be missing altogether. It has been reported from electron microscopy that the mALT contains ~288, the mlALT 88-100 and the tALT ~60 fibers from the vicinity of the AL (Tanaka et al., 2012b).

Since the standard LH (Ito et al., 2014)is not based solely on PN arborisations and we wanted to exclude neurons that simply

passed through the LH making few arborisations outside of their synaptic range. We therefore calculated an 'overlap' score between PN termini within the standard LH neuropil and potential LHN arbor:

$$f(\mathrm{i}_s, j_k) = \sum_{k=1}^{n} e^{-d^2/2\delta^2}$$

Skeletons were resampled so that we considered 'points' in the neuron at 1 µm intervals and an 'overlap score' calculated as the sum of $f(\mathrm{i}_s, j_k)$ over all points s of i. Here, i is the axonal portion of a neuron, j is the dendritic portion of a putative target, δ is the distance between two points at which a synapse might occur (e.g. 1 µm), and d is the euclidean distance between points s and k . The sum is taken of the scores between each point in i and each point in j . Neurons that did not meet a threshold score of 6000 were excluded as they only skimmed past the PN arbors. Many of the remaining skeletons seemed tangential to the LH but plausibly received direct synaptic input from PNs. A 'core' set of LHNs was defined using two thresholds, one for overlap score and another for percentage dendrite within the standard LH volume (Figure S2F).

In order to define overlapping super voxels that would divide the LH and its output zones into more intuitive anatomical sub-volumes than contiguous isotropic cubes, we first used NBLAST to cluster the axonal and dendritic sub-branches of our LHONs separately. These sub-branches were generated by calculating the Strahler order within the dendrite and removing the highest order segments. We divided these sub-branches each into 25 different clusters. Each of these clusters was then used to generate a super voxel. For each cluster, a 3-D weighted kernel density estimate was calculated based on points within the clustered sub-branches. Points were placed on the neurites at 1 µm intervals and weighted as 1 / total number of points in the cluster, so that super voxels could be directly compared. An 'inclusion' score for each LHON dendrite, LHLN arbor and PN axon analyzed within each super voxel was calculated by summing the density estimate for each point in the chosen arbor, again sampled at 1 µm intervals, and normalized by the total number of points in each arbor. A 'projection' score between LH super voxels and LH target super voxels was calculated by multiplying the average LH super voxels and LH target super voxel inclusion scores for each LHON cell type.

Immunochemistry and Imaging

Immunochemistry was as described previously (Jefferis et al., 2007 and Kohl 2013) except that we used either streptavidin Alexa-568 (ThermoFisher S-11226 1:2000) for the filled neurons with Pacific Blue (ThermoFisher P31582 1:1000) for detection of mouse anti-nc82 or streptavidin Pacific Blue (ThermoFisher S-11222 1:2000) for the filled neurons awith Alexa Fluor 568 (ThermoFisher A21144 1:1000) for detection of mouse anti-nc82.

Electrophysiology and Odor Stimulation

Electrophysiological recordings were carried out using the general approach of Wilson et al. (2004) as modified by Kohl et al. (2013). Briefly, on the day of eclosion flies were CO2 anesthetized and females of the correct genotype were selected. On the day of the experiment (1-2 days later) the fly was cold anesthetized, placed in the recording chamber, and dissected for recording as described in Kohl et al. (2013). Data acquisition was performed as previously described only a Grasshopper 14S5M camera was used and the recording electrodes were 4.5 to 7 MΩ for PNs and 6 to 8 MΩ for LHNs.

Odor stimuli were delivered via a custom odor delivery system (originally described by Kohl et al., 2013; see jefferis-lab.org/resources). The setup used for these experiments had a total of 64 channels. Unless otherwise indicated, liquid odors were diluted to 0.2% (2 microliter in 1 ml) of mineral oil (Sigma Aldrich M8410) or distilled water; solid odors were dissolved at 2mg in 1ml of solvent. A full list of odors, solvents and dilutions is provided as a supplementary spreadsheet. During stimulus presentation, a portion of the airstream was switched from a solvent control to a selected odorant. The odorized air stream was then mixed with a clean carrier air stream at a 1:8 ratio to give a notional final dilution of 2.5 x 10^{-4}. The length of the valve opening stimulus was 250 ms. All the genetic driver line combinations used for electrophysiological recording are given in Table S1.

Image Analysis

Image registration of nc82 stained brains used CMTK fully automatic intensity-based 3D image registration available at `http://www.nitrc.org/projects/cmtk` (Rohlfing and Maurer, 2003; Jefferis et al., 2007). We used the registration parameters and IS2 template brain described in Cachero et al. (2010). Brains from which recordings have been made often have higher background staining in the cortical cell body layer than the IS2 template and sometimes this results in mis-registration. We addressed this issue by using a second template brain consisting of a high background image that had been successfully registered against the IS2 template.

Neuron tracing was carried out in Amira (commercial version, FEI Visualization Sciences Group, Merignac, France) using the hxskeletonize plugin (Evers et al., 2005) or with the Simple Neurite Tracer plugin for Fiji/ImageJ (Longair et al., 2011). Neurite tracing used Simple Neurite Tracer or the Virtual Finger plugin for Vaa3D (Peng et al., 2014) on previously registered image data. Traces were then loaded into R using the `nat` package. When necessary, they were transformed between the space of the JFRC2 and IS2 template brains using the approach of Manton et al. (2014) and the `nat.flybrains` R package.

Fine scale analysis of neuronal structure was carried out using NBLAST clustering (Costa et al., 2016) as implemented in the nat.nblast R package; clustering used Ward's method as implemented in the R function `hclust`.

Analysis of electrophysiological data

Spike finding was carried out in Igor Pro using the NeuroMatic package (Jason Rothman, University College London, UK, see `http://neuromatic.thinkrandom.com`) as previously described (Kohl et al., 2013). All subsequent analysis was carried out in R using custom, open source packages (**gphys**, **physplitdata**, **physplit.analysis** – see `https://github.com/sfrechter/physplit.analysis`). Note that to ensure reproducibility, the **physplitdata** package includes every spike from our study (469 cells, 638602 spikes). We determined if cells showed a significant increase in firing to an odor, by an exact one-sided Poisson test of the number of spikes to odor and control stimuli using data from four trials per cell (**physplit.analysis** function `poissonTestOdoursSF`). We adjusted raw p values to control the false discovery rate (Benjamini and Hochberg, 1995) using R's p.adjust function; responses for a given cell-odor pair were declared significant for FDR adjusted $p < 0.01$.

Odor responses profiles for LHNs were initially manually classified defining a "physiology class" which was then cross-referenced with other properties. In order for a cell to be included in our population coding analysis it had to have trials for at least 28 odors, spiking responses to at least one odor, and identification of a specific physiology class.

Odor coding analysis

AUC Analysis

The AUC analysis measured the ability of each cell physiology class to categorize the presented odors. We defined the response of each class to each odor as the maximum of the baseline subtracted responses in the 6 time bins following odor onset. We then used these responses to compute a separate AUC score for each class as a categorizer for each of the six odor categories. Because AUC scores near 1 indicate that the response of a class is a reliable indicator of the a category while scores near 0 indicate that the absence of a response is a reliable indicator for the category, we normalized the AUC scores according to:

$$\mathrm{AUC}_{\mathrm{norm}} = \frac{1}{2}\left|\mathrm{AUC} - \frac{1}{2}\right|.$$

The resulting normalized scores indicated whether either the presence or absence of a response by a class was an indicator for an odor category. For each class we also generated 5 shuffled responses per class by randomly permuting the odor labels on the responses. We then computed the maximum normalized AUC scores across odor categories within each class, and within each of the shuffles per class. Averaging maxima over the shuffles yielded one unshuffled maximum normalized AUC score, and one shuffled one. Finally, we grouped these by the three cell groups , and performed one-sided Mann-Whitney U tests to determine the differences in the median scores.

Distribution of Odor Categorizers: We defined a class as an odor categorizer if its maximum normalized AUC score described above was greater than the 95th percentile score for the corresponding shuffled population. The fraction of such classes within each population was computed and plotted. For each class determined in this way to be an odor categorizes we recorded the category for which its normalized AUC score was highest. This gave us a measure of the distribution of categorization across the categories for each physiology class. To determine whether there was a bias in the distribution of preferred categories for each type, we examined each odor category in isolation and compared the corresponding number of categorizers in each type to the number expected by chance. We modelled the chance distribution as the Gaussian approximation to a binomial distribution for n trials (total number of categorizers for a cell type) with a success probability of 1/6 (selecting one of the six categories at random). We then computed the corresponding one-sided p-value for the observed number of categorizes of a given cell type for a given odor category. Note that this measure treats each category in isolation i.e. it does not take into account the fact that a preponderance of categorizers for one category will lead to a lack of categorizes for another.

Population Responses and Dimensionality Analysis

We compared the ensemble responses of each cell type by performing principle components analysis on the binned and temporally concatenated responses of each population to the odor set. When the responses were projected into the space of the resulting principle components, the PN responses appeared to be dominated by those to esters and aldehydes, while those of ONs were more evenly distributed among the categories. To even out the responses of the PN population to the different categories we applied a point-wise divisive normalization operation to the responses of each class. Specifically, we transformed each raw response r_{orig} according to

$$r_{\mathrm{norm}} = \frac{r_{\mathrm{orig}}^n}{r_{\mathrm{orig}}^n + s^n}.$$

The parameters n and s were optimized for each class to maximize the estimated entropy of its response distribution across all bins (including baseline) and all odors. Optimization was performed using grid search over the ranges $(1, 2)$ for n and $(1, 100)$ for s. The response entropy was computed by binning the response distribution of the class pooled across bins and odors into 21 bins and computing the entropy of the corresponding probability mass function.

Dimensionality Analysis: Following (Abbott et al. 2011), the dimensionality of the population responses for each cell type was defined as

$$d = \frac{(\sum_i \lambda_i)^2}{\sum_i \lambda_i^2},$$

where λ_i are the eigenvalues of the covariance matrix of the temporally binned responses (equivalently, the loadings in PCA analysis) after baseline subtraction and removal of the the baseline time bin for each odor response. For each cell type, 10 shuffled population responses were generated by randomly permuting the odor labels while maintaining the bin labels within each odor. The dimensionality of each cell type was compared to that of the shuffled distribution by fitting a Gaussian distribution to the shuffled distribution and computing the p-value of the observed dimensionality relative to this distribution.

Because the dimensionality score is affected by the number of classes in each type, raw dimensionality scores can not be compared across cell types. To address this, we performed a subsampling analysis in which, for each pairwise comparison of two cell types, we randomly subsampled the larger population to the size of the smaller population 10 times, yielding a dimensionality distribution. We then computed and reported the one-sided p-value of of the dimensionality of the smaller population relative to a Gaussian fit to the dimensionality distribution of the subsampled population.

Mapping categories to voxels

Each neuronal class was assigned a category by selecting the odor category with the highest AUC. We then calculated a combined voxel-category score by calculating the mean voxel score, selecting only the classes whose score was maximal for that category. This way only when classes were both specific for an odor category and had dense arborization in a specific voxel a high voxel score was generated. We then manually selected two separate thresholds for the LH and the output regions as the two distributions of voxel scores were quite different.

Electron Microscopy analysis

The whole fly brain EM dataset is described by Zheng et al. (2017) and is available for public download at `temca2data.org`. We identified some of the largest primary neurite tracts by combining bridging registrations of existing light level data (Manton et al., 2014; Zheng et al., 2017) and by simple anatomical tracing. Tract size was calculated by counting all the profiles in a single plane. For large tracts, we traced a random subset of these profiles until the first branch point and/or LH entry point – this was used to estimate the number of profiles in the tract belonging to LHNs. For those neurons whose first branch point was in the LH it was not possible to determine whether they were LHLNs or LHONs.

Preliminary work in Zheng et al. (2017) partially traced and identified most uniglomerular projection neurons. An account of the tracing of projection neuron axons in the LH including marking all their presynapses is given in Dolan et al. (2017). We completed LH arbors for excitatory uniglomerular PNs from the following 51glomeruli: D, DA1, DA2, DA3, DA4l, DA4m, DC1, DC2, DC3, DC4, DL1, DL2d, DL2v, DL3, DL4, DL5, DM1, DM2, DM3, DM4, DM5, DM6, DP1l, DP1m, V, VA1d, VA1v, VA2, VA3, VA4, VA5, VA6, VA7l, VA7m, VC1, VC2, VC3l, VC3m, VC4, VC5, VL1, VL2a, VL2p, VM1, VM2, VM3, VM4, VM5d, VM5v, VM7d, VM7v.

ACKNOWLEDGMENTS

We thank P. Hasel, B. Gyenes, G. Johnson and J. Roote for their assistance with Split-GAL4 screening. . We thank the LMB workshops for extending our odor delivery device and Jake Grimmett and Toby Darling for assistance with the LMB's compute cluster. We thank R. Roberts and P. Schlegel for contributing to EM tracing. We gratefully acknowledge the leadership of Ann-Shyn Chiang and his colleagues in sharing the latest version (1.1) of the flycircuit.tw single cell dataset. Images from FlyCircuit were obtained from the NCHC (National Center for High-performance Computing) and NTHU (National Tsing Hua University), Hsinchu, Taiwan. We acknowledge M. Landgraf, B. White, B.J. Dickson, G. Rubin, Y. Aso and the Bloomington Stock Center and the Developmental Studies Hybridoma Bank for fly stocks and antibodies. We thank R. Benton and members of the Jefferis lab for comments on the manuscript. We also thank J. Jeanne and R. Wilson for stimulating discussions and sharing results ahead of publication. This work was supported by the Medical Research Council [MRC file reference U105188491], ERC Starting (211089) and Consolidator (649111) grants and a Wellcome Collaborative Award (203261/Z/16/Z) to GSXEJ, an EMBO Young Investigator and FENS-Kavli Scholar.

References

Abbott, L., Rajan, K., and Sompolinsky, H. (2011). Interactions between Intrinsic and Stimulus-Evoked Activity in Recurrent Neural Networks, ch. 4.

Aso, Y., Grübel, K., Busch, S., Friedrich, A.B., Siwanowicz, I., and Tanimoto, H. (2009). The mushroom body of adult Drosophila characterized by GAL4 drivers. Journal of neurogenetics *23*, 156–172.

Aso, Y., Hattori, D., Yu, Y., Johnston, R.M., Iyer, N.A., Ngo, T.T., Dionne, H., Abbott, L., Axel, R., Tanimoto, H., et al. (2014a). The neuronal architecture of the mushroom body provides a logic for associative learning. eLife *3*, e04577.

Aso, Y., Sitaraman, D., Ichinose, T., Kaun, K.R., Vogt, K., Belliart-Guérin, G., Plaçais, P.Y., Robie, A.A., Yamagata, N., Schnaitmann, C., et al. (2014b). Mushroom body output neurons encode valence and guide memory-based action selection in Drosophila. eLife *3*, e04580.

Azeredo da Silveira, R., and Roska, B. (2011). Cell types, circuits, computation. Curr Opin Neurobiol *21*, 664–71.

Baden, T., Berens, P., Franke, K., Román Rosón, M., Bethge, M., and Euler, T. (2016). The functional diversity of retinal ganglion cells in the mouse. Nature *529*, 345–50.

Benjamini, Y., and Hochberg, Y. (1995). Controlling the false discovery rate: a practical and powerful approach to multiple testing. Journal of the Royal Statistical Society. Series B (Methodological) , 289–300.

Berck, M.E., Khandelwal, A., Claus, L., Hernandez-Nunez, L., Si, G., Tabone, C.J., Li, F., Truman, J.W., Fetter, R.D., Louis, M., Samuel, A.D., and Cardona, A. (2016). The wiring diagram of a glomerular olfactory system. Elife *5*.

Bhandawat, V., Olsen, S.R., Gouwens, N.W., Schlief, M.L., and Wilson, R.I. (2007). Sensory processing in the Drosophila antennal lobe increases reliability and separability of ensemble odor representations. Nat Neurosci *10*, 1474–1482.

Busch, S., Selcho, M., Ito, K., and Tanimoto, H. (2009). A map of octopaminergic neurons in the Drosophila brain. J Comp Neurol *513*, 643–67.

Cachero, S., Ostrovsky, A.D., Yu, J.Y., Dickson, B.J., and Jefferis, G.S.X.E. (2010). Sexual dimorphism in the fly brain. Curr Biol *20*, 1589–601.

Caron, S.J.C., Ruta, V., Abbott, L.F., and Axel, R. (2013). Random convergence of olfactory inputs in the Drosophila mushroom body. Nature *497*, 113–7.

Chiang, A.S., Lin, C.Y., Chuang, C.C., Chang, H.M., Hsieh, C.H., Yeh, C.W., Shih, C.T., Wu, J.J., Wang, G.T., Chen, Y.C., Wu, C.C., Chen, G.Y., Ching, Y.T., Lee, P.C., Lin, C.Y., Lin, H.H., Wu, C.C., Hsu, H.W., Huang, Y.A., Chen, J.Y., Chiang, H.J., Lu, C.F., Ni, R.F., Yeh, C.Y., and Hwang, J.K. (2011). Three-dimensional reconstruction of brain-wide wiring networks in Drosophila at single-cell resolution. Curr Biol *21*, 1–11.

Choi, G.B., Stettler, D.D., Kallman, B.R., Bhaskar, S.T., Fleischmann, A., and Axel, R. (2011). Driving opposing behaviors with ensembles of piriform neurons. Cell *146*, 1004–15.

Costa, M., Manton, J.D., Ostrovsky, A.D., Prohaska, S., and Jefferis, G.S.X.E. (2016). NBLAST: Rapid, Sensitive Comparison of Neuronal Structure and Construction of Neuron Family Databases. Neuron *91*, 293–311.

Davison, I.G., and Ehlers, M.D. (2011). Neural circuit mechanisms for pattern detection and feature combination in olfactory cortex. Neuron *70*, 82–94.

Dionne, H., Hibbard, K.L., Cavallaro, A., Kao, J.C., and Rubin, G.M. (2018). Genetic Reagents for Making Split-GAL4 Lines in Drosophila. Genetics *209*, 31–35.

Dolan, M.J., Belliart-Guerin, G., Bates, A.S., Aso, Y., Frechter, S., Roberts, R.J.V., Schlegel, P., Wong, A., Hammad, A., Bock, D., Rubin, G.M., Preat, T., Placais, P.Y., and Jefferis, G.S.X.E. (2017). Communication from learned to innate olfactory processing centers is required for memory retrieval in Drosophila. bioRxiv .

Evers, J.F., Schmitt, S., Sibila, M., and Duch, C. (2005). Progress in functional neuroanatomy: precise automatic geometric reconstruction of neuronal morphology from confocal image stacks. J Neurophysiol *93*, 2331–42.

Fişek, M., and Wilson, R.I. (2014). Stereotyped connectivity and computations in higher-order olfactory neurons. Nat Neurosci *17*, 280–8.

Frank, D.D., Enjin, A., Jouandet, G.C., Zaharieva, E.E., Para, A., Stensmyr, M.C., and Gallio, M. (2017). Early Integration of Temperature and Humidity Stimuli in the Drosophila Brain. Curr Biol *27*, 2381–2388.e4.

Frank, D.D., Jouandet, G.C., Kearney, P.J., Macpherson, L.J., and Gallio, M. (2015). Temperature representation in the Drosophila brain. Nature *519*, 358–61.

Galizia, C.G. (2014). Olfactory coding in the insect brain: data and conjectures. European Journal of Neuroscience *39*, 1784–1795.

Gruntman, E., and Turner, G.C. (2013). Integration of the olfactory code across dendritic claws of single mushroom body neurons. Nat Neurosci *16*, 1821–9.

Gupta, N., and Stopfer, M. (2012). Functional Analysis of a Higher Olfactory Center, the Lateral Horn. The Journal of Neuroscience *32*, 8138–8148.

Hallem, E.A., and Carlson, J.R. (2006). Coding of odors by a receptor repertoire. Cell *125*, 143–60.

Heimbeck, G., Bugnon, V., Gendre, N., Keller, A., and Stocker, R.F. (2001). A central neural circuit for experience-independent olfactory and courtship behavior in Drosophila melanogaster. Proc Natl Acad Sci U S A *98*, 15336–41.

Hubel, D.H., and Wiesel, T.N. (1998). Early exploration of the visual cortex. Neuron *20*, 401–12.

Ito, K., Okada, R., Tanaka, N.K., and Awasaki, T. (2003). Cautionary observations on preparing and interpreting brain images using molecular biology-based staining techniques. Microsc Res Tech *62*, 170–86.

Ito, K., Shinomiya, K., Ito, M., Armstrong, J.D., Boyan, G., Hartenstein, V., Harzsch, S., Heisenberg, M., Homberg, U., Jenett, A., Keshishian, H., Restifo, L.L., Rössler, W., Simpson, J.H., Strausfeld, N.J., Strauss, R., Vosshall, L.B., and Insect Brain Name Working Group (2014). A systematic nomenclature for the insect brain. Neuron *81*, 755–65.

Ito, M., Masuda, N., Shinomiya, K., Endo, K., and Ito, K. (2013). Systematic analysis of neural projections reveals clonal composition of the Drosophila brain. Curr Biol *23*, 644–55.

Iurilli, G., and Datta, S.R. (2017). Population Coding in an Innately Relevant Olfactory Area. Neuron *93*, 1180–1197.e7.

Jefferis, G.S.X.E., Marin, E.C., Watts, R.J., and Luo, L. (2002). Development of neuronal connectivity in Drosophila antennal lobes and mushroom bodies. Curr Opin Neurobiol *12*, 80–6.

Jefferis, G.S.X.E., Potter, C.J., Chan, A.M., Marin, E.C., Rohlfing, T., Maurer, C.R.J., and Luo, L. (2007). Comprehensive maps of Drosophila higher olfactory centers: spatially segregated fruit and pheromone representation. Cell *128*, 1187–1203.

Jenett, A., Rubin, G.M., Ngo, T.T., Shepherd, D., Murphy, C., Dionne, H., Pfeiffer, B.D., Cavallaro, A., Hall, D., Jeter, J., et al. (2012). A GAL4-Driver Line Resource for Drosophila Neurobiology. Cell reports *2*, 991–1001.

Kim, H., Kirkhart, C., and Scott, K. (2017). Long-range projection neurons in the taste circuit of Drosophila. Elife *6*.

Knaden, M., and Hansson, B.S. (2014). Mapping odor valence in the brain of flies and mice. Curr Opin Neurobiol *24*, 34–8.

Kohl, J., Ostrovsky, A.D., Frechter, S., and Jefferis, G.S.X.E. (2013). A bidirectional circuit switch reroutes pheromone signals in male and female brains. Cell *155*, 1610–23.

Laissue, P.P., Reiter, C., Hiesinger, P.R., Halter, S., Fischbach, K.F., and Stocker, R.F. (1999). Three-dimensional reconstruction of the antennal lobe in Drosophila melanogaster. J Comp Neurol *405*, 543–52.

Lee, P.C., Chuang, C.C., Chiang, A.S., and Ching, Y.T. (2012). High-throughput computer method for 3D neuronal structure reconstruction from the image stack of the Drosophila brain and its applications. PLoS Comput Biol *8*, e1002658.

Lee, T., and Luo, L. (1999). Mosaic analysis with a repressible cell marker for studies of gene function in neuronal morphogenesis. Neuron *22*, 451–461.

Lee, Y.H., Lin, Y.N., Chuang, C.C., and Lo, C.C. (2014). SPIN: a method of skeleton-based polarity identification for neurons. Neuroinformatics *12*, 487–507.

Lin, H.H., Lai, J.S.Y., Chin, A.L., Chen, Y.C., and Chiang, A.S. (2007). A map of olfactory representation in the Drosophila mushroom body. Cell *128*, 1205–1217.

Litwin-Kumar, A., Harris, K.D., Axel, R., Sompolinsky, H., and Abbott, L.F. (2017). Optimal Degrees of Synaptic Connectivity. Neuron *93*, 1153–1164.e7.

Longair, M.H., Baker, D.A., and Armstrong, J.D. (2011). Simple Neurite Tracer: open source software for reconstruction, visualization and analysis of neuronal processes. Bioinformatics *27*, 2453–4.

Luan, H., Peabody, N.C., Vinson, C.R., and White, B.H. (2006). Refined spatial manipulation of neuronal function by combinatorial restriction of transgene expression. Neuron *52*, 425–36.

Luo, S.X., Axel, R., and Abbott, L.F. (2010). Generating sparse and selective third-order responses in the olfactory system of the fly. Proc Natl Acad Sci U S A *107*, 10713–8.

Manton, J.D., Ostrovsky, A.D., Goetz, L., Costa, M., Rohlfing, T., and Jefferis, G.S.X.E. (2014). Combining genome-scale Drosophila 3D neuroanatomical data by bridging template brains. Bioarxiv preprint .

Marin, E.C., Jefferis, G.S., Komiyama, T., Zhu, H., and Luo, L. (2002). Representation of the Glomerular Olfactory Map in the Drosophila Brain. Cell *109*, 243–255.

Masland, R.H. (2001). Neuronal diversity in the retina. Curr Opin Neurobiol *11*, 431–6.

Masse, N.Y., Turner, G.C., and Jefferis, G.S.X.E. (2009). Olfactory information processing in Drosophila. Curr Biol *19*, R700–13.

Milyaev, N., Osumi-Sutherland, D., Reeve, S., Burton, N., Baldock, R.A., and Armstrong, J.D. (2012). The Virtual Fly Brain browser and query interface. Bioinformatics *28*, 411–5.

Miyamichi, K., Amat, F., Moussavi, F., Wang, C., Wickersham, I., Wall, N.R., Taniguchi, H., Tasic, B., Huang, Z.J., He, Z., Callaway, E.M., Horowitz, M.A., and Luo, L. (2011). Cortical representations of olfactory input by trans-synaptic tracing. Nature *472*, 191–6.

Münch, D., and Galizia, C.G. (2016). DoOR 2.0–Comprehensive Mapping of Drosophila melanogaster Odorant Responses. Sci Rep *6*, 21841.

Murthy, M., Fiete, I., and Laurent, G. (2008). Testing odor response stereotypy in the Drosophila mushroom body. Neuron *59*, 1009–1023.

Okada, R., Awasaki, T., and Ito, K. (2009). Gamma-aminobuyric acid (GABA)-mediated neural connections in the Drosophila antennal lobe. J Comp Neurol *514*, 74–91.

Olsen, S.R., Bhandawat, V., and Wilson, R.I. (2007). Excitatory Interactions between Olfactory Processing Channels in the Drosophila Antennal Lobe. Neuron *54*, 89–103.

Ostrovsky, A., Cachero, S., and Jefferis, G. (2013). Clonal analysis of olfaction in Drosophila: image registration. Cold Spring Harb Protoc *2013*, 347–9.

Panser, K., Tirian, L., Schulze, F., Villalba, S., Jefferis, G.S.X.E., Bühler, K., and Straw, A.D. (2016). Automatic Segmentation of Drosophila Neural Compartments Using GAL4 Expression Data Reveals Novel Visual Pathways. Curr Biol *26*, 1943–1954.

Papadopoulou, M., Cassenaer, S., Nowotny, T., and Laurent, G. (2011). Normalization for sparse encoding of odors by a wide-field interneuron. Science *332*, 721–5.

Patella, P., and Wilson, R.I. (2018). Functional Maps of Mechanosensory Features in the Drosophila Brain. Curr Biol *28*, 1189–1203.e5.

Peng, H., Tang, J., Xiao, H., Bria, A., Zhou, J., Butler, V., Zhou, Z., Gonzalez-Bellido, P.T., Oh, S.W., Chen, J., Mitra, A., Tsien, R.W., Zeng, H., Ascoli, G.A., Iannello, G., Hawrylycz, M., Myers, E., and Long, F. (2014). Virtual finger boosts three-dimensional imaging and microsurgery as well as terabyte volume image visualization and analysis. Nat Commun *5*, 4342.

Perez-Orive, J., Mazor, O., Turner, G.C., Cassenaer, S., Wilson, R.I., and Laurent, G. (2002). Oscillations and sparsening of odor representations in the mushroom body. Science *297*, 359–65.

Priebe, N.J., and Ferster, D. (2012). Mechanisms of neuronal computation in mammalian visual cortex. Neuron *75*, 194–208.

Rohlfing, T., and Maurer, C. R., J. (2003). Nonrigid image registration in shared-memory multiprocessor environments with application to brains, breasts, and bees. IEEE Trans Inf Technol Biomed *7*, 16–25.

Root, C.M., Denny, C.A., Hen, R., and Axel, R. (2014). The participation of cortical amygdala in innate, odour-driven behaviour. Nature *515*, 269–73.

Roy, B., Singh, A.P., Shetty, C., Chaudhary, V., North, A., Landgraf, M., Vijayraghavan, K., and Rodrigues, V. (2007). Metamorphosis of an identified serotonergic neuron in the Drosophila olfactory system. Neural Dev *2*, 20.

Ruta, V., Datta, S.R., Vasconcelos, M.L., Freeland, J., Looger, L.L., and Axel, R. (2010). A dimorphic pheromone circuit in Drosophila from sensory input to descending output. Nature *468*, 686–90.

Schlegel, P., Costa, M., and Jefferis, G.S. (2017). Learning from connectomics on the fly. Curr Opin Insect Sci *24*, 96–105.

Seki, Y., Aonuma, H., and Kanzaki, R. (2005). Pheromone processing center in the protocerebrum of Bombyx mori revealed by nitric oxide-induced anti-cGMP immunocytochemistry. J Comp Neurol *481*, 340–51.

Shang, Y., Claridge-Chang, A., Sjulson, L., Pypaert, M., and Miesenbock, G. (2007). Excitatory local circuits and their implications for olfactory processing in the fly antennal lobe. Cell *128*, 601–612.

Shekhar, K., Lapan, S.W., Whitney, I.E., Tran, N.M., Macosko, E.Z., Kowalczyk, M., Adiconis, X., Levin, J.Z., Nemesh, J., Goldman, M., McCarroll, S.A., Cepko, C.L., Regev, A., and Sanes, J.R. (2016). Comprehensive Classification of Retinal Bipolar Neurons by Single-Cell Transcriptomics. Cell *166*, 1308–1323.e30.

Sosulski, D.L., Bloom, M.L., Cutforth, T., Axel, R., and Datta, S.R. (2011). Distinct representations of olfactory information in different cortical centres. Nature *472*, 213–6.

Stensmyr, M.C., Dweck, H.K.M., Farhan, A., Ibba, I., Strutz, A., Mukunda, L., Linz, J., Grabe, V., Steck, K., Lavista-Llanos, S., Wicher, D., Sachse, S., Knaden, M., Becher, P.G., Seki, Y., and Hansson, B.S. (2012). A conserved dedicated olfactory circuit for detecting harmful microbes in Drosophila. Cell *151*, 1345–57.

Sterling, P., and Laughlin, S. (2015). Principles of Neural Design (MIT Press).

Stettler, D.D., and Axel, R. (2009). Representations of odor in the piriform cortex. Neuron *63*, 854–64.

Strutz, A., Soelter, J., Baschwitz, A., Farhan, A., Grabe, V., Rybak, J., Knaden, M., Schmuker, M., Hansson, B.S., and Sachse, S. (2014). Decoding odor quality and intensity in the Drosophila brain. Elife *3*, e04147.

Tanaka, N.K., Awasaki, T., Shimada, T., and Ito, K. (2004). Integration of chemosensory pathways in the Drosophila second-order olfactory centers. Curr Biol *14*, 449–57.

Tanaka, N.K., Endo, K., and Ito, K. (2012a). Organization of antennal lobe-associated neurons in adult Drosophila melanogaster brain. Journal of Comparative Neurology *520*, 4067–4130.

Tanaka, N.K., Suzuki, E., Dye, L., Ejima, A., and Stopfer, M. (2012b). Dye fills reveal additional olfactory tracts in the protocerebrum of wild-type Drosophila. J Comp Neurol *520*, 4131–40.

Tanaka, N.K., Tanimoto, H., and Ito, K. (2008). Neuronal assemblies of the Drosophila mushroom body. Journal of Comparative Neurology *508*, 711–755.

Tasic, B., Menon, V., Nguyen, T.N., Kim, T.K., Jarsky, T., Yao, Z., Levi, B., Gray, L.T., Sorensen, S.A., Dolbeare, T., Bertagnolli, D., Goldy, J., Shapovalova, N., Parry, S., Lee, C., Smith, K., Bernard, A., Madisen, L., Sunkin, S.M., Hawrylycz, M., Koch, C., and Zeng, H. (2016). Adult mouse cortical cell taxonomy revealed by single cell transcriptomics. Nat Neurosci *19*, 335–46.

Technau, G., and Heisenberg, M. (1982). Neural reorganization during metamorphosis of the corpora pedunculata in Drosophila melanogaster. Nature *295*, 405–407.

Tirian, L., and Dickson, B. (2017). The VT GAL4, LexA, and split-GAL4 driver line collections for targeted expression in the Drosophila nervous system. bioRxiv .

Turner, G.C., Bazhenov, M., and Laurent, G. (2008). Olfactory representations by Drosophila mushroom body neurons. J Neurophysiol *99*, 734–46.

Venken, K.J.T., Simpson, J.H., and Bellen, H.J. (2011). Genetic manipulation of genes and cells in the nervous system of the fruit fly. Neuron *72*, 202–30.

Wang, Y., Chiang, A.S., Xia, S., Kitamoto, T., Tully, T., and Zhong, Y. (2003). Blockade of neurotransmission in Drosophila mushroom bodies impairs odor attraction, but not repulsion. Curr Biol *13*, 1900–4.

Wang, Y., Guo, H.F., Pologruto, T.A., Hannan, F., Hakker, I., Svoboda, K., and Zhong, Y. (2004). Stereotyped odor-evoked activity in the mushroom body of Drosophila revealed by green fluorescent protein-based Ca2+ imaging. J Neurosci *24*, 6507–14.

Wang, Y., Pu, Y., and Shen, P. (2013). Neuropeptide-gated perception of appetitive olfactory inputs in Drosophila larvae. Cell Rep *3*, 820–30.

Wilson, R.I., and Laurent, G. (2005). Role of GABAergic inhibition in shaping odor-evoked spatiotemporal patterns in the Drosophila antennal lobe. J Neurosci *25*, 9069–79.

Wilson, R.I., and Mainen, Z.F. (2006). Early events in olfactory processing. Annu Rev Neurosci *29*, 163–201.

Wilson, R.I., Turner, G.C., and Laurent, G. (2004). Transformation of olfactory representations in the Drosophila antennal lobe. Science *303*, 366–70.

Wong, A.M., Wang, J.W., and Axel, R. (2002). Spatial representation of the glomerular map in the Drosophila protocerebrum. Cell *109*, 229–41.

Yorozu, S., Wong, A., Fischer, B.J., Dankert, H., Kernan, M.J., Kamikouchi, A., Ito, K., and Anderson, D.J. (2009). Distinct sensory representations of wind and near-field sound in the Drosophila brain. Nature *458*, 201–5.

Yu, H.H., Awasaki, T., Schroeder, M.D., Long, F., Yang, J.S., He, Y., Ding, P., Kao, J.C., Wu, G.Y.Y., Peng, H., Myers, G., and Lee, T. (2013). Clonal development and organization of the adult Drosophila central brain. Curr Biol *23*, 633–43.

Zeng, H., and Sanes, J.R. (2017). Neuronal cell-type classification: challenges, opportunities and the path forward. Nat Rev Neurosci *18*, 530–546.

Zheng, Z., Lauritzen, J.S., Perlman, E., Robinson, C.G., Nichols, M., Milkie, D., Torrens, O., Price, J., Fisher, C.B., Sharifi, N., Calle-Schuler, S.A., Kmecova, L., Ali, I.J., Karsh, B., Trautman, E.T., Bogovic, J., Hanslovsky, P., Jefferis, G.S.X.E., Kazhdan, M., Khairy, K., Saalfeld, S., Fetter, R.D., and Bock, D.D. (2017). A Complete Electron Microscopy Volume Of The Brain Of Adult Drosophila melanogaster. bioRxiv .

FIGURES

Figure 1

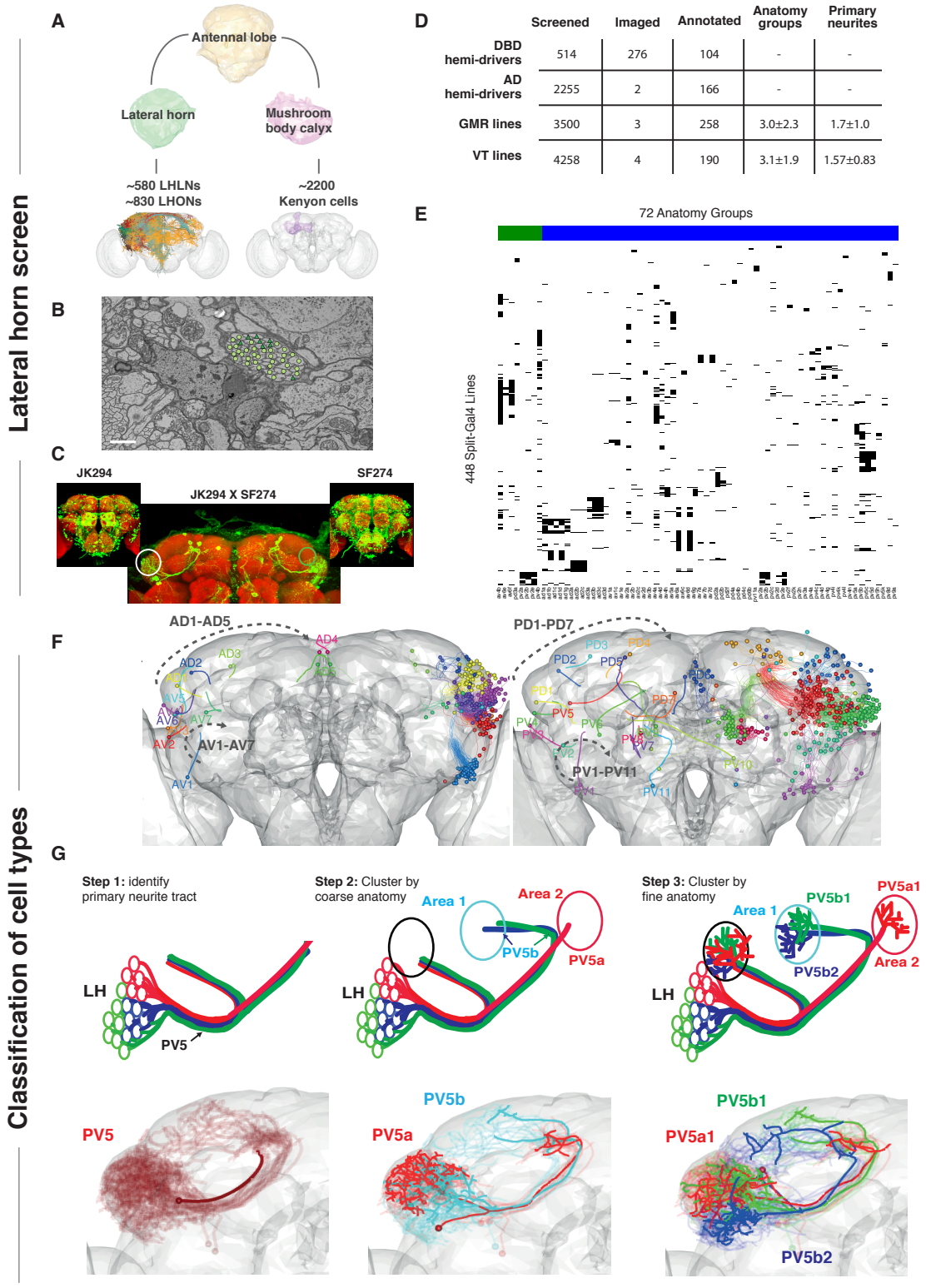

	Screened	Imaged	Annotated	Anatomy groups	Primary neurites
DBD hemi-drivers	514	276	104	-	-
AD hemi-drivers	2255	2	166	-	-
GMR lines	3500	3	258	3.0±2.3	1.7±1.0
VT lines	4258	4	190	3.1±1.9	1.57±0.83

Figure 1: **Screen for genetic driver lines labeling Lateral Horn Neurons**
(A) Flow diagram following flow of olfactory information to third order neurons of the LH and MB calyx. **(B)** A section through the PV5 primary neurite tract within the EM data, demonstrating separating the neurons to LHNs (circles) and non LHNs (triangles). Scale bar 1 µm. **(C)** Sample Split-GAL4 intersections; inset show the parental lines. Cell body locations marked with a white circle. **(D)** Summary table for the genetic screen **(E)** Matrix describing the different lines and clusters. The clusters are grouped and colored LHON=Blue, LHLN=Green. **(F)** Front and posterior view of the different primary tracks into the LH. Black arrow indicates the order of labeling of the different primary tracts. **(G)** Upper, a cartoon demonstrating the logic of the naming system with, lower, the PV5 primary neurite as an example. For simplicity we only used 3 out of the cell types in PV5.

Tract	Type	Profiles	Est. LHNs	Range
AV3	LHON>LHLN	144	140	140
PD2	LHON	193	128	128
PV5	LHON	127	119	119
AD1	LHON	286	116	102 - 130
AV6	LHON	323	106	96 - 115
AV2	LHON>>LHLN	98	63	49 - 77
AD3	LHON	59	59	59
AV7	LHON	141	48	25 - 70
AV1	LHON	33	25	25
AV5	LHON	108	17	7 - 27
PV3	LHON	52	12	0 - 25
AD2	LHON	52	0	0
	–LHONs–	1616	832	797 - 868
AV4	LHLN>>LHON	324	252	244 - 259
PV4	LHLN>LHON	158	155	152 - 158
PV2	LHLN>>LHON	193	92	81 - 102
PD3	LHLN	75	59	43 - 75
PD4	LHLN	88	22	10 - 33
	–LHLNs–	838	578	555 - 602
	–All–	2454	1411	1368 - 1454

Table 1: **LHN tracts characterized in electron microscopy data** (Related to Figure 1)
Tracts match the Primary Neurite Tract nomenclature defined in Figure 1. Type indicates whether the tract contains output or local neurons. Profiles indicates the total number of profiles within the tract. Est. LHNs indicates the sampling based estimate for the number of LHNs in the tract. Range gives a 90% confidence interval.

Figure 2

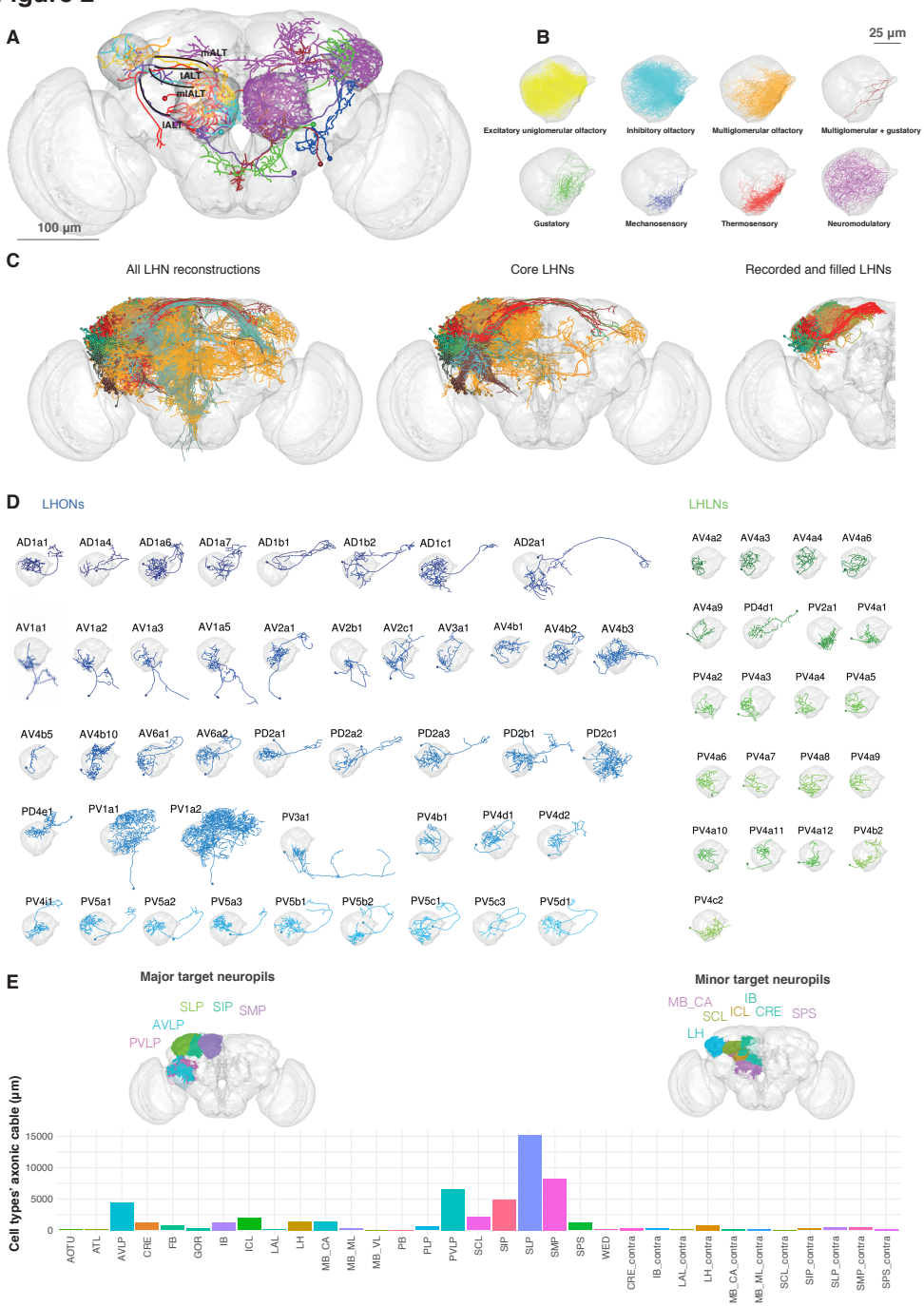

Figure 2: **Single cell anatomy of the Lateral Horn**
(A) Sample single projection neurons with axonal projections in the LH, showing all major axon tracts and sensory modalities that provide input. **(B)** Close up of the LH in which the axonal arbors for all FlyCircuit neurons of each presumptive sensory modality displayed. **(C)** Overview of our annotated LHN skeleton library showing all skeletons with LH arbors, core LHN cell types (see Figure S2) and those neurons reconstructed after electrophysiological recording in the present study. Neurons colored by anatomy group. **(D)** Visualization of single exemplars for all cell types for which we have >=3 skeletons in the library, or from which we made electro-physiological recordings in this study. Output neurons in blue, local neurons in green. **(E)** Bar chart showing, for each target neuropil, the total axonal cable length contributed by all core LHONs (calculated as sum of mean for each identified cell type). Brains plots show in major (> 3 mm axonal cable) and minor (1-3 mm) targets of LHONs. Brain neuropil according to Ito et al. (2014); contra, contralateral, ipsi, ipsilateral. mALT, medial antennal lobe tract, tALT, transverse antennal lobe tract, mlALT, medio-lateral antennal lobe tract, lALT, lateral antennal lobe tract, LHONs, lateral horn output neurons, LHLNs, lateral horn local neurons.

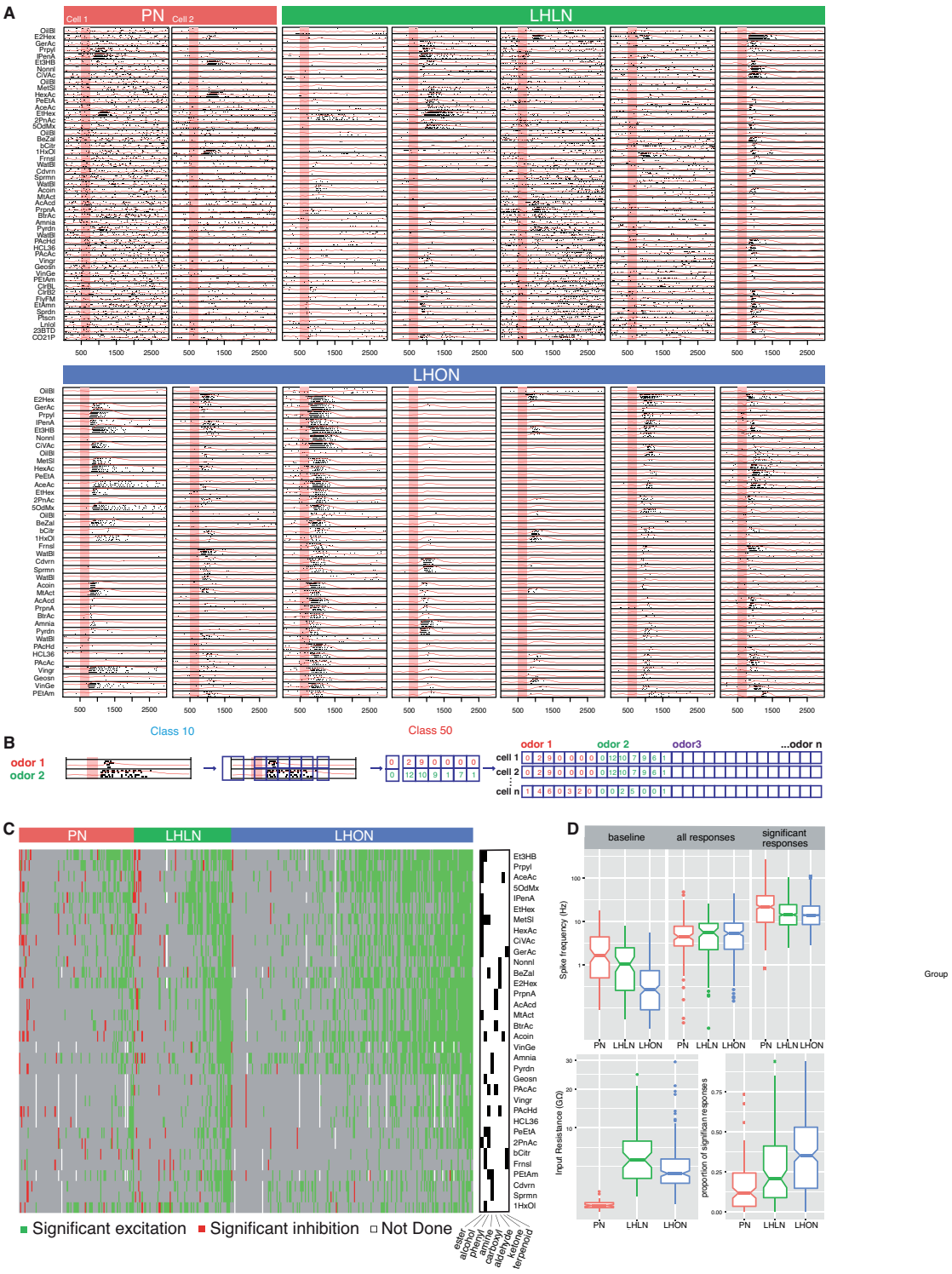

Figure 3: **Odor responses of LHNs**

(A) Examples of responses of different cell types. The top panel show a couple of PN responses (red) and different LHLN types (green) for comparison to responses of different LHON types (Blue) in the bottom panel. Each odor was presented 4 times **(B)** A cartoon description of our physiology pipeline for presentation and analysis. Each odor was presented 4 times. For presentation the voltage response (red line) is the average voltage across the 4 odor prsentations. First the spiking response for each odor are stacked and then responses of each cell to the different odors are stacked again. For analysis the responses of each cell to the different odors ware concatenated into one continuous vector **(C)** Matrix describing significant responses of the different cells (PNs LHLNs and LHONs labeled by the same colors as above) to the different odors. A black and white matrix shows the functional groups of the different odors. **(D)** Comparing basic cell/response properties of PN LHLN and LHOns. Top panel: baseline firing rate (baseline), firing rate in the response window (all responses), and firing rate in the response window for significant responses only (significant responses). Bottom Panel: Input resistance and proportion of significant responses.

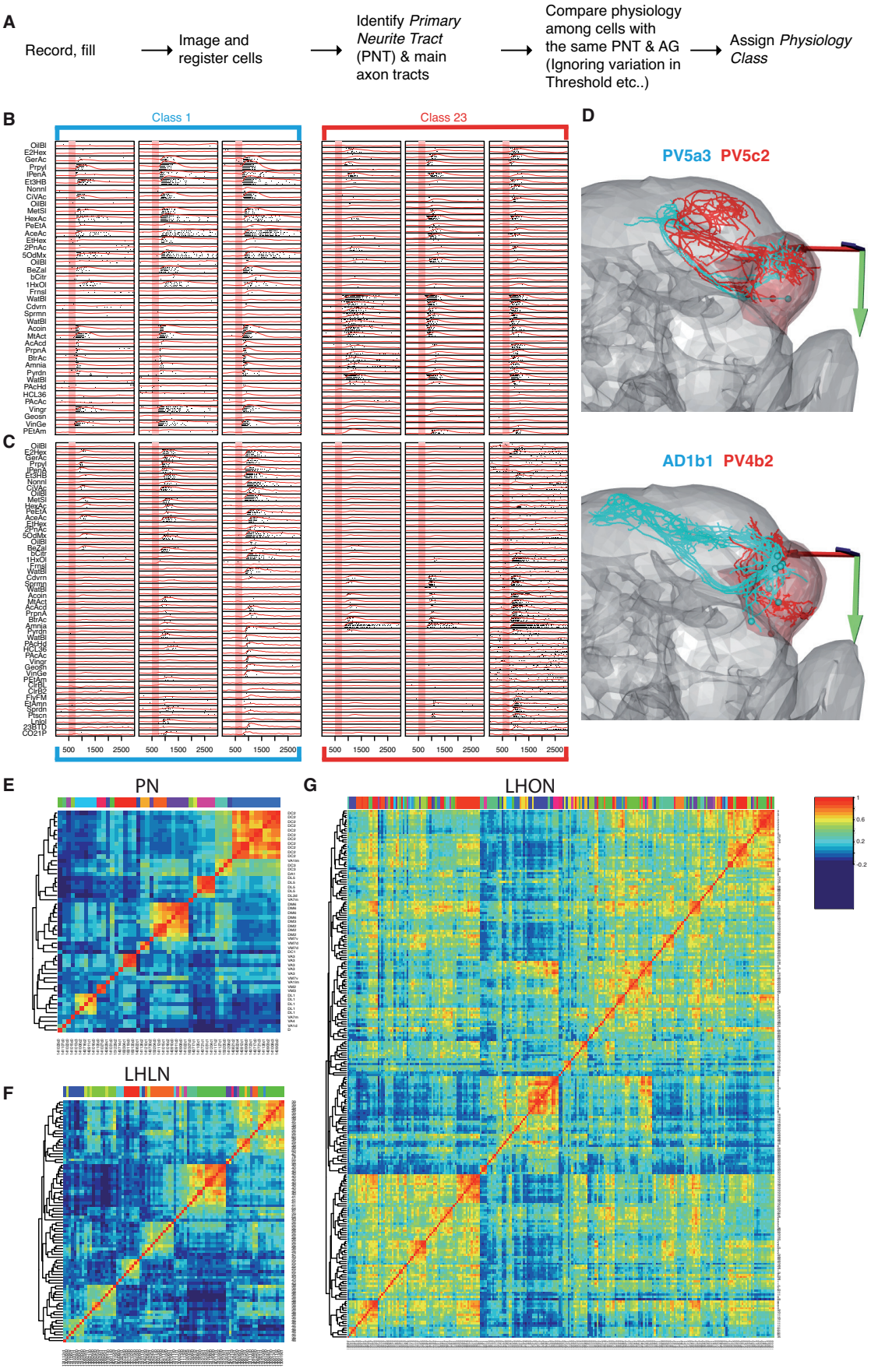

Figure 4:
(A) Our pipeline for manually assigning physiology classes for the cells **(B)** Examples of responses of different cell that belong to the same class. Shown are two relatively simple cases where the similarity between the responses is easily identified.ßHeatmaps for PN LHLN LHON odor responses. **(C)** Examples of responses of different cell that belong to the same class. Shown are two less obvious cases where there is a significant variability in the strength of the response For comparison all three matrices share the same color scale (see **)** (**D**) Projections of the traced cells that belong to the physiology classes in B and C **(E-G)** Heatmaps for PN, LHLNs trand LHONs odour responses. For comparison all three matrices share the same color scale (right).

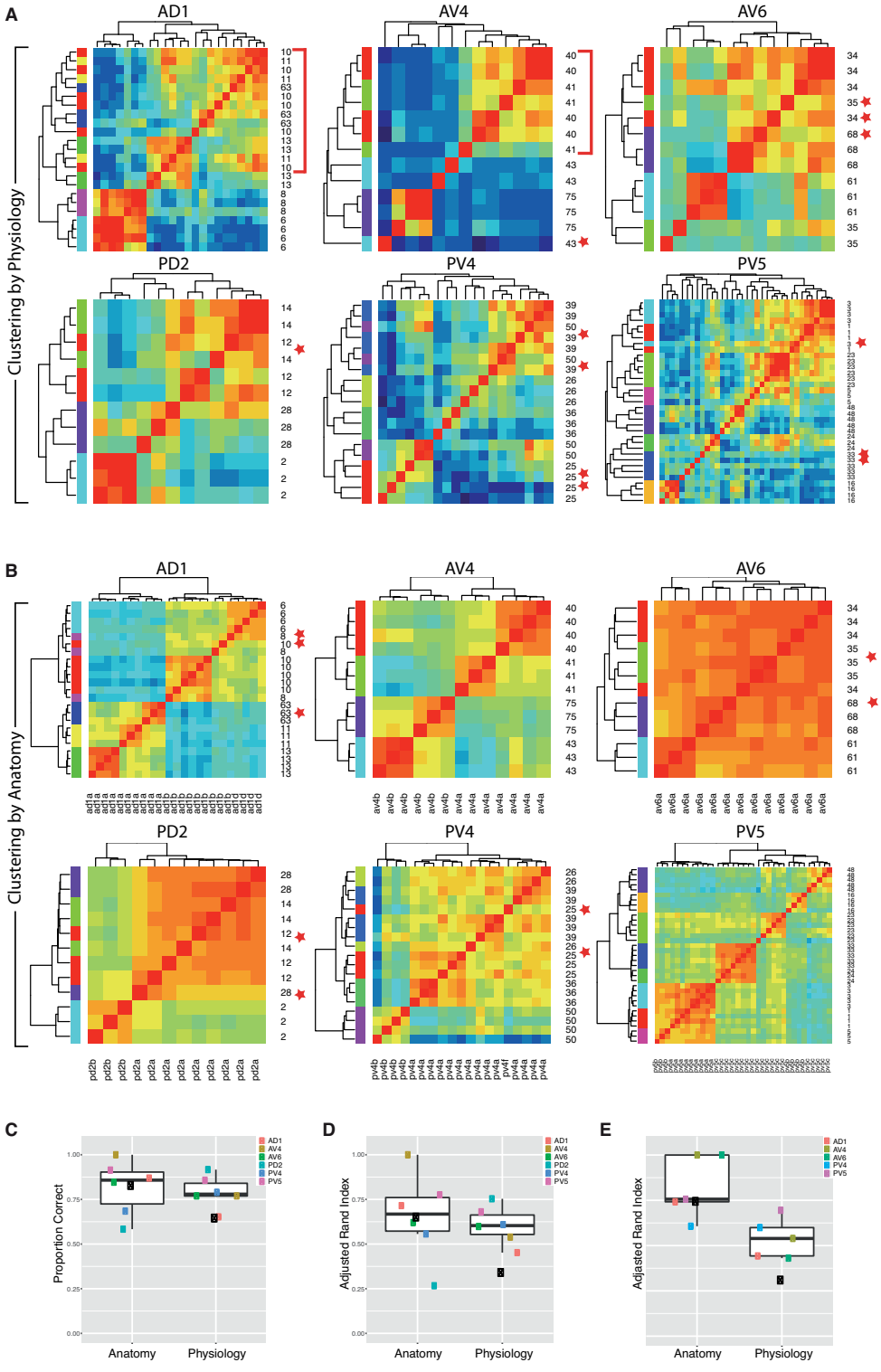

Figure 5:
(A) Cross correlation matrix of odor responses for all the traced cells divided according to their PNT **(B)** Anatomy Cross correlation matrix of all the cells in A **(C)** Summary comparing percent correct clustering score for each primary neurite tract by physiology and anatomy **(D)** Summary comparing Adjusted Rand Index clustering score for each primary neurite tract by physiology and anatomy **(E)** Summary comparing percent correct clustering score for each primary neurite tract by physiology and anatomy after correcting class labels in two cases (and removing PD2).

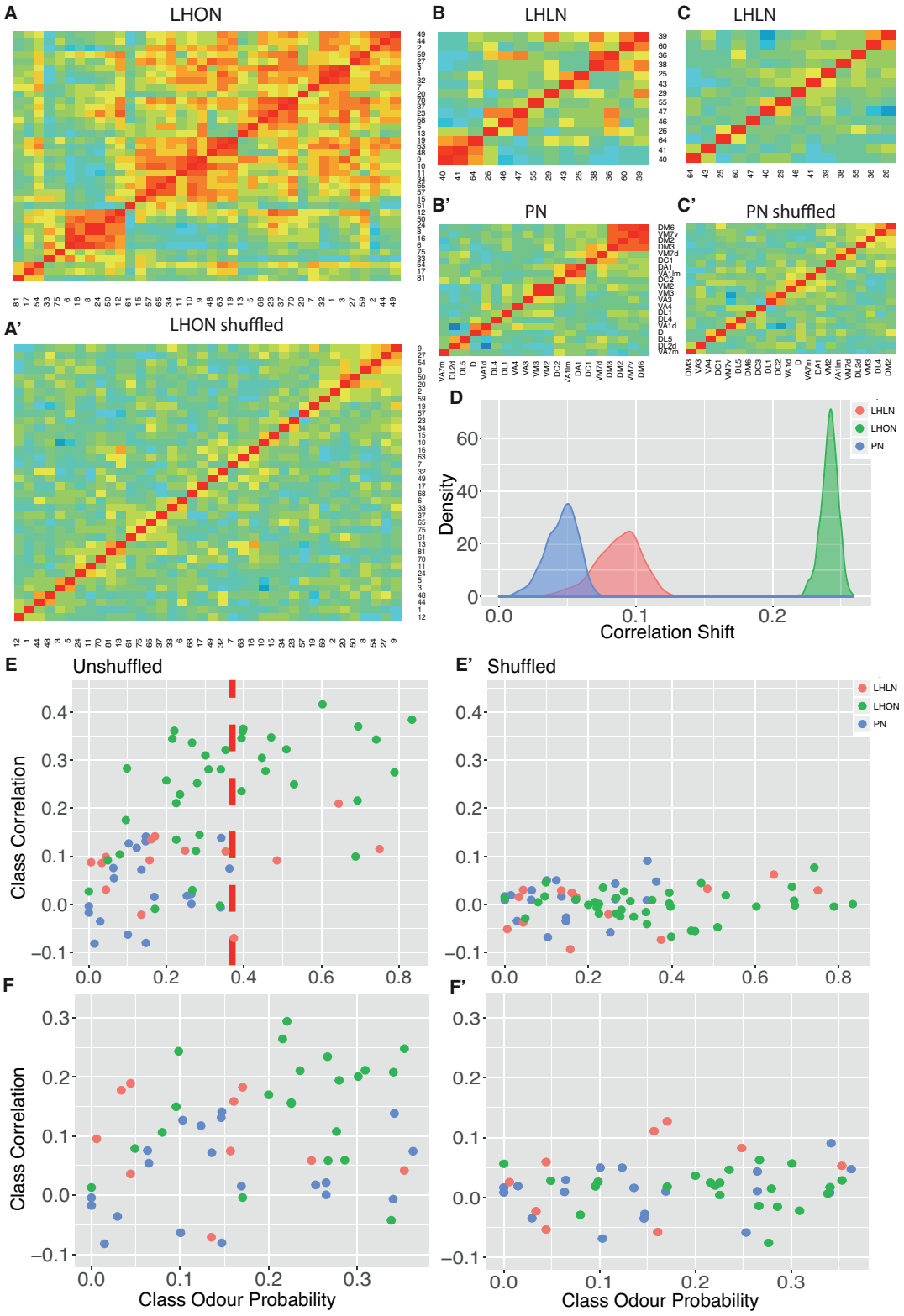

Figure 6:
LHON (A) LHLN (B) and PN (C) heatmap of odor responses after aggregation by physiology class**.** The same after randomizing the odor labels for LHON (A') LHLN (B') and PN (C') . (D) Histogram of mean correlation shift by randomizing the odor labels for each of the groups. (E) Class correlation plotted against class mean frequency of significant responses. For each class the correlation to all the other classes in the group was calculated before **(E)** and after **(E')** odor label shuffling. (F) Same as E. Only correlation between sparse cells (left to red line in E) was considered.

Figure 7

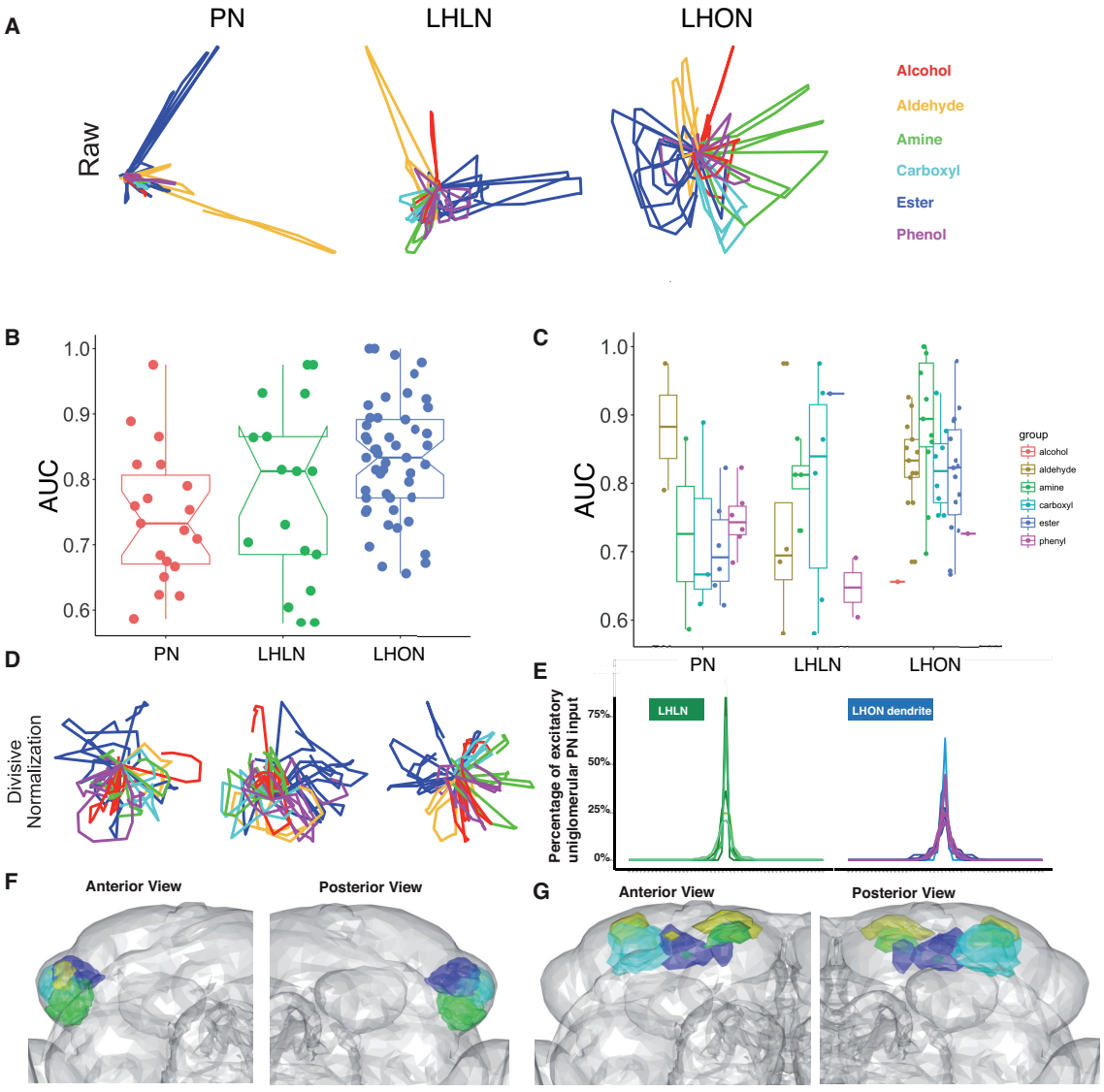

Figure 7: LHONs are better odor categorizers than their input
(A) Population representations of odors. Responses are projected into the spaces of the second and third principal components, and color-coded by odor category. **(B)** Distribution of AUC scores for PNs and LHLNs and LHONs. An AUC score of 0.5 indicates no information about odor category. Box=25-75% centiles, line=median, whiskers 5-95% centiles, notch indicates bootstrap 95% confidence interval of the median. LHON odor responses convey more category information than PNs ($p < 0.005$), one-sided Mann-Whitney U-test. **(C)** Distribution of AUC scores for each population divided into the different odor categories **(D)** PCA analysis after divisive normalization. (**E**) Input tuning curves for a set of 6 LHLNs and 13 LHONs. Each line is single LHN. The x axis is rank ordered by the number of synaptic inputs from uniglomerular PNs from each of 51 glomeruli. **(F)** Mapping of the different odor categories to voxels (see methods:Odor coding analysis)

SUPPLEMENTAL INFORMATION

Supplemental Experimental Procedures

Online resources

The online resources provided in the paper are listed at http://jefferislab.org/si/.

Supplemental Figures

Cross name	AD	DBD	Cross name	AD	DBD
JK834SF478	SF478	JK834	JK1730Cha	Cha	JK1730
JK2204SF478	SF478	JK2204	JK1593Cha	Cha	JK1593
JK1473SF478	SF478	JK1473	JK1473Cha	Cha	JK1473
JK1091SF478	SF478	JK1091	JK1354Cha	Cha	JK1354
JK2204SF431	SF431	JK2204	JK1168Cha	Cha	JK1168
JK1473SF431	SF431	JK1473	JK1109Cha	Cha	JK1109
JK1473SF406	SF406	JK1473	JK1091Cha	Cha	JK1091
JK843-SF401	SF401	JK843	JK1029Cha	Cha	JK1029
JK843-SF341	SF341	JK843	JK1011Cha	Cha	JK1011
JK1742SF341	SF341	JK1742	EG21Cha	Cha	EG21
JK2324SF281	SF281	JK2324	GMRMB486B-SplitGal4 G	GMR_48H12	GMR_54F05
SF274JK671	SF274	JK671	GMRSS01144-SplitGal4 G	GMR_22A02	GMR_115F09
SF274JK512	SF274	JK512	NP7217-Gal4		
SF274JK304	SF274	JK304	NP6099-Gal4		
SF274JK294	SF274	JK294	MZ671-Gal4		
SF274JK1742	SF274	JK1742	MZ19-Gal4		
JK843SF232	SF232	JK843	InSite0089-Gal4		
JK814SF232	SF232	JK814	GMR85E04-Gal4		
JK627SF230	SF230	JK627	GMR71D08-Gal4		
JK627SF214	SF214	JK627	GMR66B12-Gal4		
JK627SF158	SF158	JK627	GMR65D05-Gal4		
JK946SF131	SF131	JK946	GMR51B07-Gal4		
JK627SF131	SF131	JK627	GMR30H02-Gal4		
JK814SF127	SF127	JK814	GMR19E02-Gal4		
JK627SF127	SF127	JK627	GMR17G11-Gal4		
JK801Cha	Cha	JK801	GMR16C09-Gal4		
JK705Cha	Cha	JK705	GMR12F11-Gal4		
JK56Cha	Cha	JK56	GMR11G08-Gal4		
JK2402Cha	Cha	JK2402	GMR11E08-Gal4		
JK2227Cha	Cha	JK2227	GH146-Gal4		
JK2204Cha	Cha	JK2204			

Table S1: **LHN tracts characterized in electron microscopy data** (Related to Figure 1)
A table of all the insertion lines used for electrophysiology. For Split Gal4 lines the AD and DBD are also added.

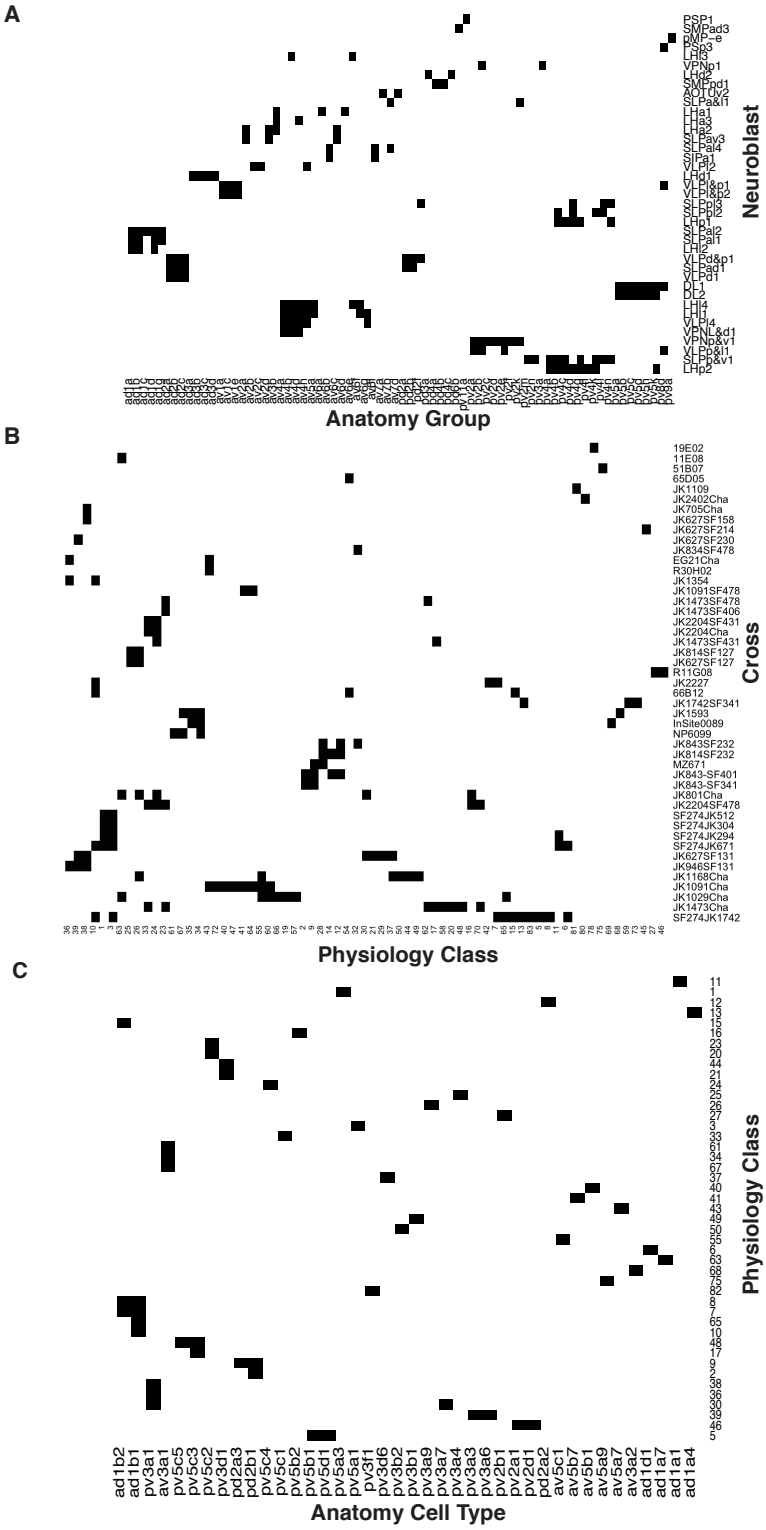

Figure S1: **Computational anatomy SI** (Related to Figure 2)
(A) Matrix showing putative neuroblast origin for anatomy groups identified in the screen. **(B)** Matrix showing physiology classes together with the cross they were recorded from **(C)** Matrix connecting each of the physiology classes with an anatomy cell types it belong to.

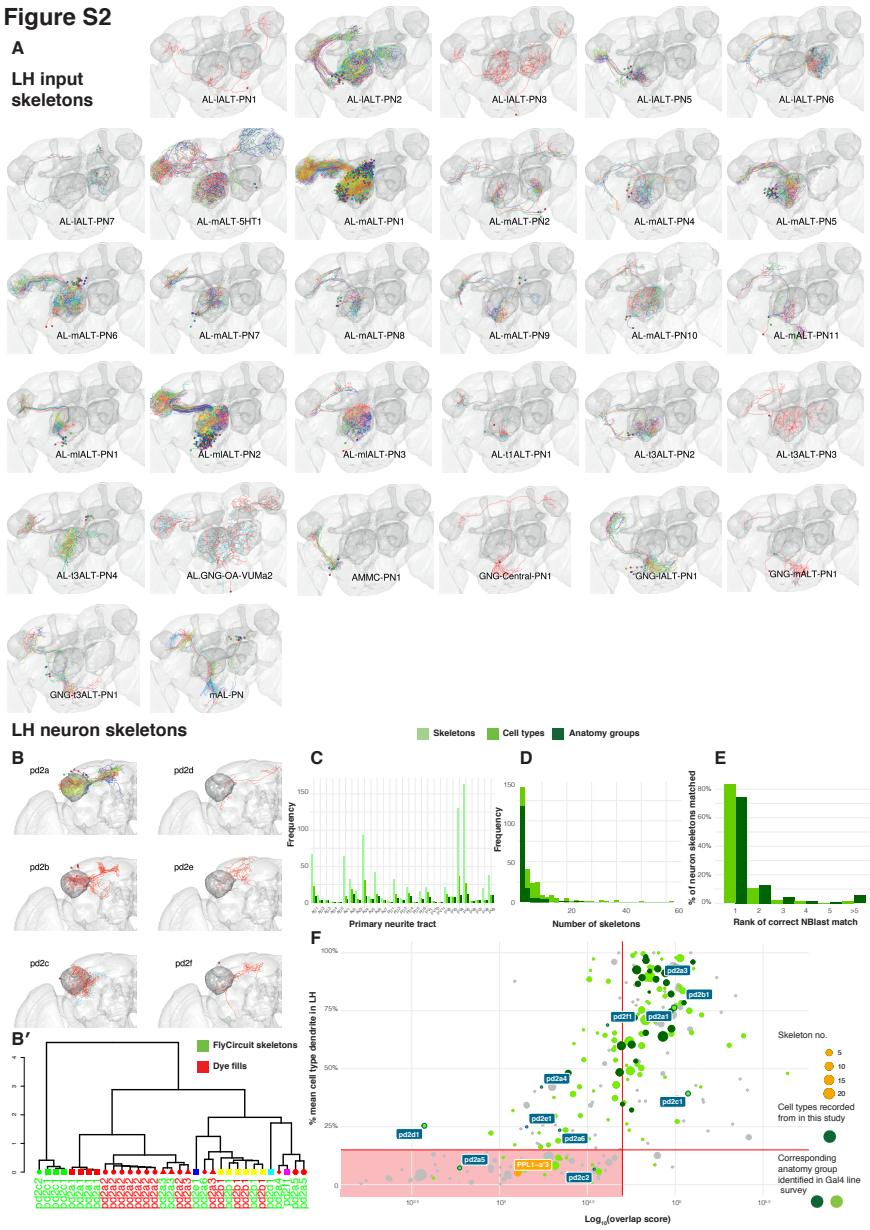

Figure S2: **Summary of neuron skeleton data for LHNs and PNs** (Related to Figure 2)
(A) FlyCircuit PN skeletons shown co-registered in a standard brain, broken down into separate anatomy groups (panels). Individual skeletons in different colors. The number of skeletons is indicative of the number of single cell clones in FlyCircuit, and may not directly relate to the number of cell in the brain. LH, MB lobes and AL shown in a darker grey. **(B)** Example of an LHN primary neurite cluster, PD2. The is cluster broken down into its constituent anatomy groups (panels) and cell types (colors). **(B')** Using NBLAST to disambiguate cell types and anatomy groups. Dendrogram represents a hierarchical clustering of NBLAST scores. Node shape and color indicate different anatomy groups. Leaf color indicates the origin of each skeleton; FlyCircuit dataset or dye-fills from the present study. **(C)** The number of skeletons, cell types and anatomy groups in the LHN dataset in each primary neurite cluster. **(D)** Histogram showing the number of skeletons in, and therefore used to define, the LHN anatomy groups and cell types. **(E)** Using NBLAST to match a neuron skeleton to the correct anatomy group. Each skeleton in the dataset was removed and then NBLASTed against the rest, mean scores were taken per anatomy group, and anatomy groups ranked. Bar chart shows the percentage of skeletons matched to, 1, the correct anatomy group and, >=2, incorrect anatomy groups. **(F)** Defining a 'core' set of LHNs. Scatter plot shows cell type plotted against the Log10 of their overlap score (see Methods) with PN termini and the proportion of their dendritic arbor (see Methods) in the standard LH (Ito et al., 2014). Horizontal decision boundary at 15%, vertical decision boundary at 50000, red box, non 'core' LHNs. The dopaminergic MB input neuron, PPL1-a'3 (Aso et al., 2014a), is flagged in orange as an example of a non-core LHON. Points bounded in blue indicate cell types shown in panel A. Points in chartreuse and dark green indicate cell types belonging to anatomy groups that have been identified in a screen of Gal4 lines in this study. Electrophysiological recordings have been taken from the cell types in dark green in the present study.

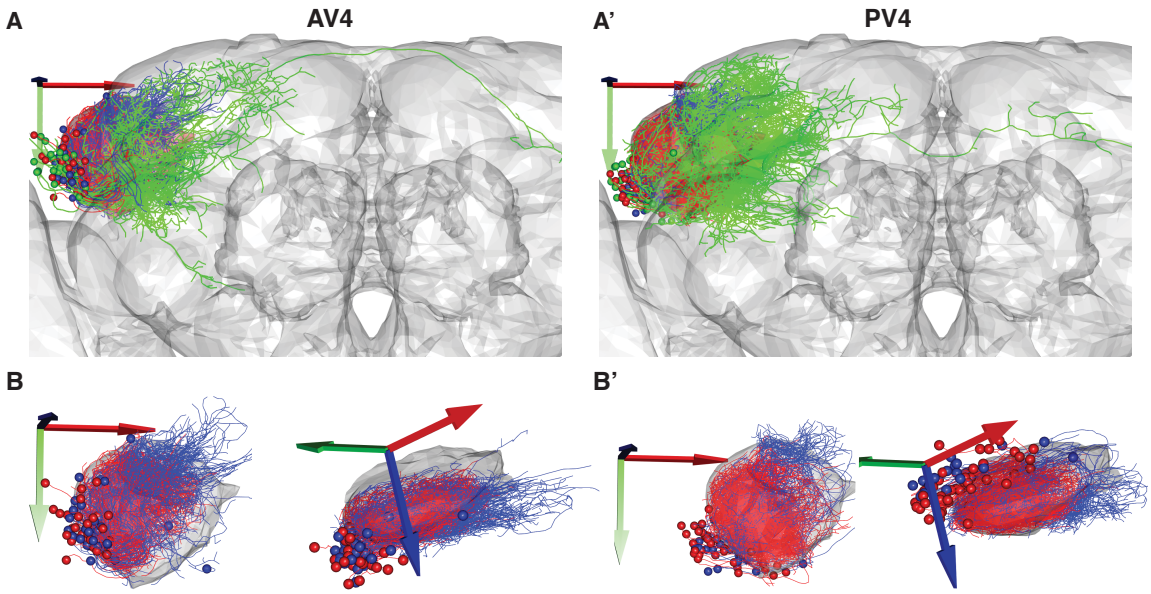

Figure S3: **LocalOutputNeuroanatomy** (Related to Figure 2)
(A) frontal view of the 2 largest tracts containing local interneurons. Local anatomy group AV4a (A') and PV4a (A") are colored red. Similar clusters with arborization outside the LH AV4b (A') and PV4b (A') are colored blue. The rest of the anatomy groups in these primary neurite tracts are colored green. **(B)** Same as A but showing frontal and dorsolateral views with the two main local anatomy groups only.

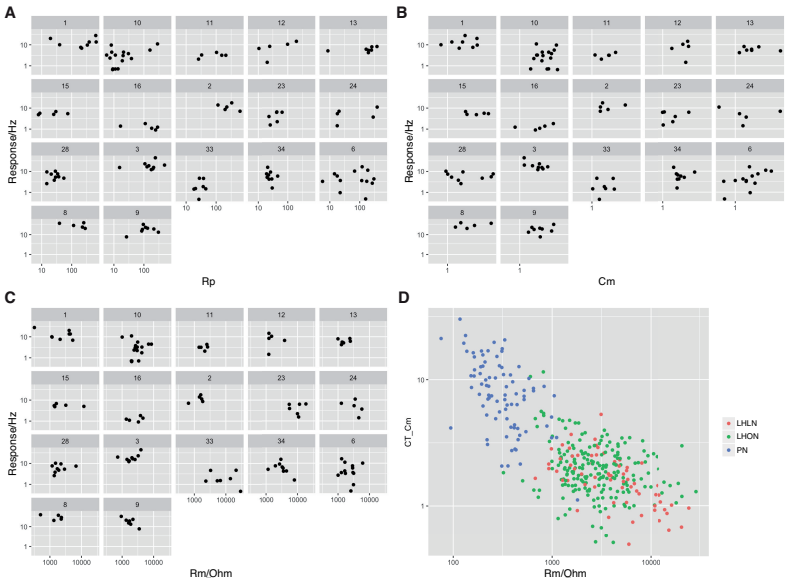

Figure S4: (related to Figure 4)
For each physiology class the mean response is plotted against the access resistance (A), the cell capacitance (B), and the membrane resistance (C). Cell capacitance is plotted against the membrane resistance. cells ara collored according to their group

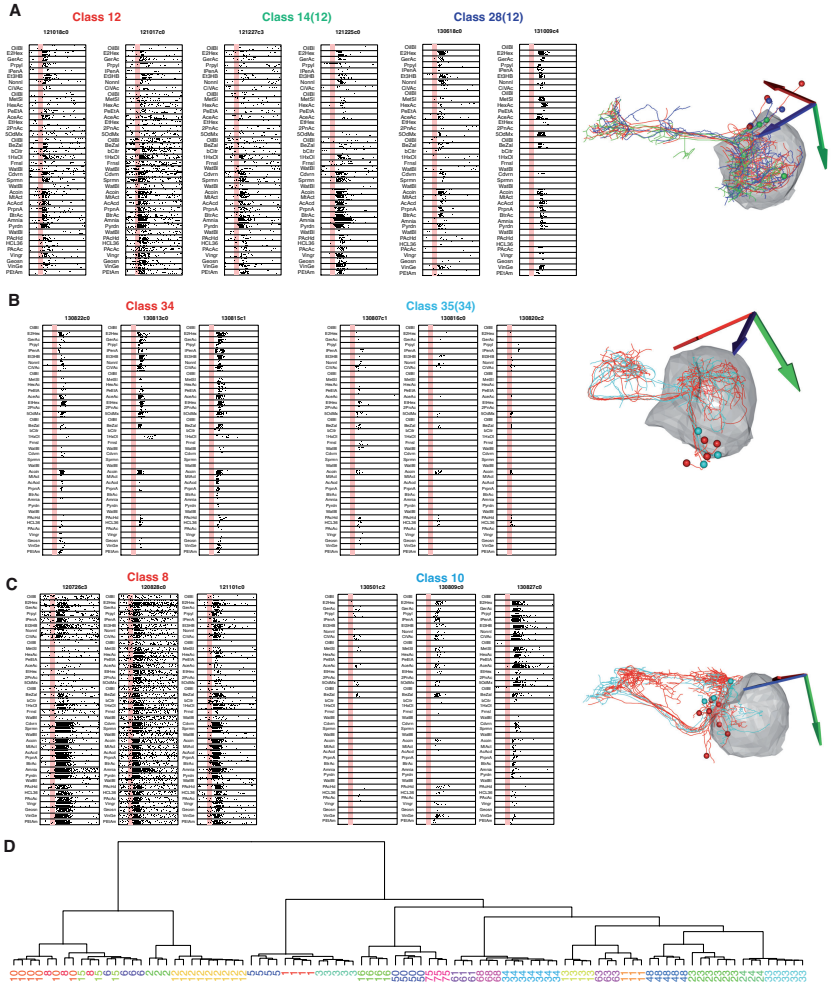

Figure S5: (related to Figure 5)
We identified 4 cases in which both odor tuning and anatomy had significant similarities **(A,B)** Classes 24 and 33 and classes 6 and 8 are similar both in physiology and anatomy but yet significant differences enable identification . **(C,D)** Both couples of classes 12,28 and 34,35 are similar both in physiology and anatomy and we cannot be 100% sure that are actually different cell types. **(E)** Replotting of the anatomy dendrogram after reassigning the merged classes